CEAS Aeronautical Journal (2022) 13:535–557
https://doi.org/10.1007/s13272-022-00579-1

ORIGINAL PAPER

Comparison and evaluation of blade element methods against RANS simulations and test data

Ole Bergmann[1] · F. Götten[1] · C. Braun[1] · F. Janser[1]

Received: 8 March 2021 / Revised: 21 December 2021 / Accepted: 3 March 2022 / Published online: 5 April 2022

Abstract

This paper compares several blade element theory (BET) method-based propeller simulation tools, including an evaluation against static propeller ground tests and high-fidelity Reynolds-Average Navier Stokes (RANS) simulations. Two proprietary propeller geometries for paraglider applications are analysed in static and flight conditions. The RANS simulations are validated with the static test data and used as a reference for comparing the BET in flight conditions. The comparison includes the analysis of varying 2D aerodynamic airfoil parameters and different induced velocity calculation methods. The evaluation of the BET propeller simulation tools shows the strength of the BET tools compared to RANS simulations. The RANS simulations underpredict static experimental data within 10% relative error, while appropriate BET tools overpredict the RANS results by 15–20% relative error. A variation in 2D aerodynamic data depicts the need for highly accurate 2D data for accurate BET results. The nonlinear BET coupled with XFOIL for the 2D aerodynamic data matches best with RANS in static operation and flight conditions. The novel BET tool PropCODE combines both approaches and offers further correction models for highly accurate static and flight condition results.

Keywords BET · CFD propeller simulation · Propeller aerodynamics · Actuator disk modelling · Propeller performance

Abbreviations

AoA	Angle of attack
BET	Blade element theory
CFD	Computational fluid dynamics
J	Advance ratio
LLT	Lifting line theory
RANS	Reynolds-averaged Navier–Stokes
Re	Reynolds number
RPM	Revolution per minute

Latin

a_a	Axial induction factor (–)
A_{Prop}	Propeller area (m^2)
a_t	Tangential induction factor (–)
b	Quadratic behaviour factor (–)
C_{chord}	Chord length (m)
c_{d_α}	Drag coefficient as function of AoA (–)
c_{d_0}	Drag coefficient at zero AoA (–)
c_{l_α}	Lift coefficient as function of AoA (–)
c_{l_0}	Lift coefficient at zero AoA (–)
D	Drag (N)
f	Reynolds scaling exponent (–)
FM	Figure of merit (–)
L	Lift (N)
N_{Blades}	Number of blades (–)
P	Power (W)
Q	Torque (N m)
R	Propeller radius (m)
r	Local radius (m)
T	Thrust (N)
u	Circumferential velocity (m/s)
v_∞	Free stream velocity (m/s)
w	Relative velocity (m/s)
w_a	Axial velocity (m/s)
w_t	Tangential velocity (m/s)

Greek

α	Effective angle of attack (rad)
β	Propeller twist (rad)
η	Efficiency (–)
Γ	Circulation (m^2/s)
$\omega_{Propeller}$	Angular velocity (1/s)
ϕ	Helix angle (rad)
ρ	Density (kg/m^3)

✉ Ole Bergmann
bergmann@fh-aachen.de

[1] Department of Aerospace Engineering, FH Aachen University of Applied Sciences, Hohenstaufenallee 6, Aachen, Germany

Subscripts

′	Section coefficients/section loads
r	Local radius dependency
ref	Reference value
0	Zero angle of attack

1 Introduction

Renewed attention is paid to propellers' design and performance prediction to the increasing market of electrically driven urban air mobility (UAM) [1]. Fully electric and hybrid electric air mobility solutions are assumed to have the potential to reduce aircraft noise [2]. Furthermore, electrically driven aeroplanes can reduce greenhouse emissions if renewable energy sources are used. Thus, hybrid or even fully electric aerial vehicles will enter the market in the near term to reach Flightpath 2050s emission reduction targets [3]. Research into the implementation of electric and hybrid electric drive systems is proceeding apace [4–6].

Any electric air mobility solutions use propellers for propulsion and lift enhancement or implement vertical take-off and landing capabilities. In the case of UAM applications, hover efficiency and noise emission drives propeller or rotor design [7]. Therefore, accurate performance prediction in hover condition, which is equivalent to low advance ratio condition or static test condition, is necessary. Nevertheless, propeller simulation tools have to predict flight performance or high advance ratio conditions accurately. Particularly tiltrotor applications require both low and high advance ratio thrust and performance estimations for maximal hover efficiency and sufficient horizontal flight performance [8, 9]. Therefore, this work identifies the best open-source simulation tool to predict hover performance and high-speed performance.

In general, three categories of estimation methods are commonly used. First, highly accurate and highly complex Reynolds-averaged Navier–Stokes (RANS) based propeller simulations are used. RANS requires significant computational power, particularly for low advance ratio conditions. However, RANS simulations provide detailed information about the flowfield and resulting forces. Second, low-fidelity simulations are less accurate in detail but need a fraction of the computational power of RANS simulations. The low fidelity simulation methods need to be understood appropriately for a thorough interpretation of results. However, with a sufficient understanding of the flow phenomena, propeller design is feasible with low-fidelity simulation techniques [10]. Blade element theories (BET) are accurate and cost-efficient simulation techniques. BET are typically coupled with a momentum approach or a lifting line theory (LLT) to improve accuracy [11, 12]. Finally, analytical and empirical models can be used for performance estimations. Still, these models are out of the scope of this paper as they are unsuitable for detailed propeller analysis and off-design performance prediction. Analytical models are derived from the general momentum theory but do not capture friction losses, among other things. According to ESDU [13, 14] or Hamilton Standard [15], empirical models can predict propeller performance and general propeller planform parameters. Recent studies show the strength of such models in predicting aircraft performance [16–18]. Since empirical models are not appropriate for the detailed prediction of force distributions required for aeroelastic and aeroacoustic computations, they are not further analysed in this study.

We compared five open source available low-fidelity propeller simulation tools to find the best tool suitable for low and high advance ratios. This paper gives a comprehensive overview of the most common tools and compares prediction results. The following BET-based methods are the most cited and used open propeller analysis tools, except for the in-house development for further influence studies.

- JavaProp [19]
- XROTOR [20]
- JBlade [21]
- RAALF [22]
- PropCODE

PropCODE—"Propeller comprehensive optimisation and design environment" is an in-house development for propeller aeroacoustics and aeroelastic simulation. In PropCODE different induced velocity prediction methods can be selected and are compared in this paper. In addition, the influence of varying 2D airfoil polars on the total lift and drag is analysed with PropCODE, and the importance of high fidelity 2D data is shown. The variation of the induced velocity prediction methods or the manipulation of 2D data is only possible with PropCODE.

Current literature lacks a comprehensive review and a holistic validation of the most common propeller design tools. Partial method guidelines and validation studies exist for specific propellers and applications [21, 23–26], but a general comparison between different simulation environments is unavailable. However, various studies validate BET using exist with wind tunnel data, static test data, or high-resolution RANS solutions. Still, most studies focus on small unmanned aerial vehicles rotors with diameters up to 0.5 m [27]. These rotors operate in different Reynolds number regions as required for manned flight vehicles, so they cannot be used to validate bigger full-scale propellers or rotors. However, full-scale propellers are challenging to analyse in wind tunnels, why fewer validation cases exist. Validation of full-scale propellers in large wind tunnels is only available for high-speed applications, but these tests exclude the static cases [28–30].

The presented paper combines novel static test data for validation purposes in low advance ratio region with high fidelity RANS simulations. The validated RANS simulations are further used to validate the low order tools in higher advance ratio regions.

The evaluation of this study's results helps to understand the limitations of the introduced tools for manned flight vehicles. The variation of the prediction methodology in PropCODE in low and high advance ratio conditions allows selecting a methodology for tilt–rotor or tilt–wing applications. It supports selecting an appropriate tool or methodology for the simulation of low and high advance ratio conditions. Finally, the paper presents a weighting between simulation effort, ease of use, and simulation accuracy.

2 Numerical methods

Propeller simulation can be performed with low-fidelity blade element theories (BET), high-fidelity Reynolds-averaged Navier–Stokes (RANS), or medium fidelity vortex panel methods. This paper compares and validates low-fidelity and high-fidelity simulation methodologies with static test bench data.

2.1 Low-fidelity simulation methods

The low-fidelity BET is the method of choice for unducted open propeller performance prediction in the early design stages. The simulation procedure is fast, robust and reliable in a specific range of applications. The BET is reliable in moderate loading conditions and for reduced complexity geometries, which means low sweep, low lean and moderate number of blades [31, 32]. The limitations are related to 3D flow effects and stall behaviour of the propeller blades [33]. These effects are challenging to capture with low-fidelity simulation procedures.

2.1.1 Basic theory for BET simulation

The propeller is sliced in the radial direction into 2D airfoil sections for applying the BET. It is assumed that each 2D propeller section acts as an infinite wing. With information about the velocity relative to the airfoil section, 2D aerodynamic data and the angle of attack (AoA), the 2D airfoil forces can be calculated, considering Reynolds number and Mach number dependent effects. Glauert [34] is often cited as the father of BET in the classical form, but the procedure is also used in variation by other authors. The local AoA, tangential, and axial induced velocity (wt, wa) are calculated by different schemes, for example, vortex sheets in the wake, with a lifting line procedure (LLT) or with a combined general momentum theory and BET approach.

With the predicted vectorial velocities and the 2D airfoil section data, lift and drag coefficients of the airfoil section can be calculated. The 2D lift coefficients c_{l_α} and drag coefficients c_{d_α}, depending on the effective AoA α, are used to calculate the section lift (L') and section drag (D') of the blade element. L' and D' are transformed into section thrust (T') segments and section force segments in the propeller plane (Q'). As shown in Fig. 1, T' and Q' are normal and tangential forces relative to the propeller axis and are integrated over the span to obtain the final thrust and multiplied by the section radius to obtain the final torque. For structural analysis of straight propeller, the torsional moment along the propeller blade is required, which could be provided by the moment coefficient of the 2D airfoil data. In addition, structural and aerodynamic sweep and lean effects must be addressed for structural analysis of curved propellers. Sweep and lean correction models can simply be implemented in BET methods. Lift and drag forces act in the blade section's aerodynamic centre (AC). The induced velocities w_a and w_t result from the acting forces on the fluid and distortion of the streamlines.

The described procedure is stated in the equations below:

$$L' = \frac{\rho}{2} \cdot w^2 \cdot c_{l\alpha} \cdot C_{\text{chord}}, \tag{1}$$

$$D' = \frac{\rho}{2} \cdot w^2 \cdot c_{d\alpha} \cdot C_{\text{chord}}, \tag{2}$$

$$T' = L' \cdot \cos(\phi) - D' \cdot \sin(\phi), \tag{3}$$

$$Q' = L' \cdot \sin(\phi) + D' \cdot \cos(\phi), \tag{4}$$

$$T = N_{\text{Blades}} \cdot \int_{R_{\text{Hub}}}^{R_{\text{Tip}}} T'_r \mathrm{d}r, \tag{5}$$

$$Q = N_{\text{Blades}} \cdot \int_{R_{\text{Hub}}}^{R_{\text{Tip}}} Q'_r \cdot r \mathrm{d}r. \tag{6}$$

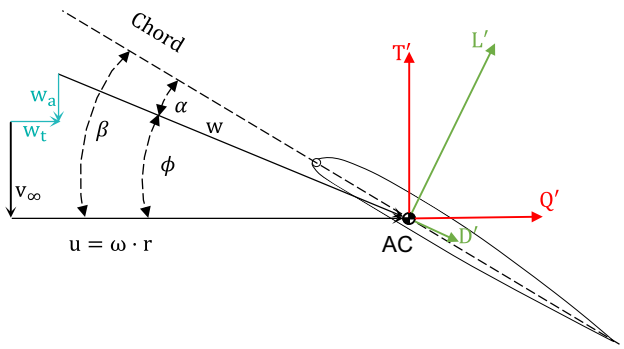

Fig. 1 Velocities and forces at a 2D blade section

C_{chord} denotes the chord of the propeller section, which is usually a function of the radius. Equation 7 provides the relationship between torque Q angular velocity $\omega_{\text{Propeller}}$ and power consumption P. Using power consumption, flight velocity v_∞ and thrust, the efficiency η is calculated (Eq. 8):

$$P = Q \cdot \omega_{\text{Propeller}}, \tag{7}$$

$$\eta = \frac{v_\infty \cdot T}{P}. \tag{8}$$

However, the efficiency results from the predicted thrust and power consumption. Therefore, errors in thrust or power accumulate in the efficiency. Second, the efficiency is zero by definition in hover conditions, which this publication focuses on. For hover conditions, the figure of merit (FM) is used to describe the rotor efficiency. The FM measures for the kinetic energy in the wake of the rotor related to the input power. A_{Prop} denotes the propeller disk area in Eq. 9. Again, errors in thrust and power consumption prediction are accumulated. Therefore, the FM is not used for comparison in this publication:

$$\text{FM} = \frac{T}{2P}\sqrt{\frac{T}{\rho \cdot A_{\text{Prop}}}}. \tag{9}$$

The BETs' advantage is the fast and robust calculation scheme for conventional propeller geometries with an accuracy of ± 15% relative error compared to experimental data [21, 25]. In addition, various correction methods could easily be implemented due to the model's reduced complexity, as described in Ref. [31]. Implemented correction models depend on the blade form and the application, e.g., a compressor blade operates under entirely different conditions than a wind turbine blade or a marine propeller. Therefore, different models have to be implemented to increase the accuracy, depending on the flow effects, for example, tip loss correction models, post-stall models, 3D correction models, compressibility models, sweep and lean models or wake correction models. Intense research about different modelling approaches and models is performed by Gur [25, 35, 36]. Therefore, this paper does not focus on the modelling approach but rather on different applications and implementations.

2.1.2 2D airfoil data

BET always needs 2D aerodynamic data as an input to calculate thrust, power, and efficiency.

In most simulation tools, 2D airfoil analysis tools like JavaFoil [37] or XFOIL [38] are used for gathering 2D airfoil polars. Both tools are 2D inviscid potential solvers, corrected with viscid models. The viscid models influence the airfoil's pressure distribution and provide capabilities to estimate stall behaviour. Subsequently, lift and pressure drag change due to the viscous boundary layer model and a friction drag estimation model are incorporated. Furthermore, compressibility models for compressible pure subsonic operations are implemented in the 2D solvers. In addition, transition models are used to estimate the laminar-turbulent transition. JavaFoil has different transition models incorporated, affecting the laminar-turbulent transition and stall behaviour [37, 39, 40].

Alternative sources for 2D coefficients are wind tunnel tests or 2D RANS simulations. Wind tunnel tests are sensitive to the measurement accuracy and the turbulence of the wind tunnel. In addition, the similarity parameters Reynolds number, Mach number, and the geometric similarity must be ensured, and two-dimensional flow conditions are required in the wind tunnel. Still, flow separation and post-stall behaviour could be measured if the similarity parameters match. RANS simulations are fast and reliable for the linear region. However, flow separation and post-stall behaviour need more computational effort, because these flow effects must be solved with an unsteady solver and high-density meshes.

The simulation accuracy of 2D aerodynamic data directly affects the BET method's results. The following table gives an overview of the 2D data handing in the BET tools. All tools, except XROTOR, import airfoil polars as discrete points with information about the AoA, lift, and drag coefficient. XROTOR needs a transformation of the 2D data in a mathematical description. XROTOR has no interface to XFOIL.

XROTOR uses the following formulation for the 2D incompressible airfoil drag and needs some basic parameters, which can be obtained from discrete polars. The lift coefficient polar is split into a linear pre-stall region and a linear post-stall region. For pre- and post-stall, the lift slope is required as well as the zero-lift angle, the maximum lift and the stall AoA. The incompressible drag polars are described by a parabolic function as stated below:

$$c_{d,\text{XROTOR}} = \left[c_{d_0} + b\left(c_{l_0} - c_l\right)^2\right]\left(\frac{\text{Re}}{\text{Re}_{\text{ref}}}\right)^f, \tag{10}$$

$$b = \frac{dc_d}{dc_l^2}. \tag{11}$$

The Reynolds number scaling exponents have to be selected with respect to the target Reynolds number, as stated in the table below. The reference Reynolds number is equal to the initial Reynolds number selected for the calculations. The values are published in Ref. [41] (Table 1).

The coefficient b is a value of the quadratic behaviour of the airfoil. Compressibility is simulated by a simple drag rise model and Prandtl–Glauert's compressibility correction [42]. The drag rise model requires the critical Mach number, which the following equation obtains according to Ref. [43] (Table 2):

$$\mathrm{Ma}_{\mathrm{crit,2D}} = 0.95 - 0.1 \cdot c_{\mathrm{l}_{\mathrm{max}}} - t/c. \tag{12}$$

This paper uses the experimental results as a reference for the simulation of the XROTOR airfoil polars.

RANS Simulations are time-consuming but are valid in the linear region [44–46] for most airfoils. XFOIL and JavaFoil results have to be validated with RANS simulations or high-accuracy wind tunnel tests. The different 2D aerodynamic data sources are compared against 2D RANS simulations performed according to the procedure of Ref. [44, 47]. As explained in Ref. [44], the 2D RANS airfoil simulations are performed with a segregated flow solver with the reliable "SST (Menter) K-ω" turbulence model [48] and the "Gamma Re Theta" transition model [49]. A specific transition model should be selected to simulate the laminar transition and better match wind tunnel data and simulation. XFOIL and JavaFoil have different transition models incorporated. For validation purposes, the same e^n approach is used in XFOIL and JavaFoil [34, 45] described in Ref. [46]. Further information about the mesh resolution could be obtained from Ref. [44].

The 2D aerodynamic data of XFOIL, JavaFoil, and RANS simulation are compared with wind tunnel tests published in Ref. [50–52]. The first comparative case is a symmetric NACA 0015 airfoil at a Reynolds number of 680,000. The second comparative case is a natural laminar flow airfoil called Somers Maughmer 701 (SM 701), originally developed for sailplane applications. The SM 701 airfoil is simulated at a Reynolds number of 1,000,000. The JavaFoil simulations are performed with a smooth surface finish, the Eppler stall model, and the e^n transition model [53], which is also used in XFOIL.

In the first case, the lift coefficient from XFOIL and JavaFoil differs from the experimental results and the RANS simulation (see Fig. 2) by a Δc_{l} of 0.1 which is equivalent to 10% at an AoA of 10°. RANS and experiment match perfectly except in the post-stall region. A slight difference could be seen at an AoA of 15.5° between the RANS simulation and experiment. RANS predicts a smoother flow detachment than measured in the experiment, resulting in higher lift coefficients for the same AoA. Reasons could be imperfections in the wind tunnel tests or an underprediction of the separation bubble.

JavaFoil overpredicts the zero-lift drag by around 35% (see Fig. 3). On the other hand, XFOIL underpredicts the drag coefficient at higher AoA slightly more than JavaFoil. RANS matches experimental results in the region around the minimum drag. A derivation of the RANS drag prediction is observed at a lift coefficient of 0.81, where the drag is decreased compared to the equivalent lift coefficient of the experimental data, and a kink in the RANS polar is present, while the experimental results increases without a kink.

The XROTOR lift polar is based on the experimental data. Therefore, a perfect matching between XROTOR data and experiment in the linear region is visible. The stall region is described by a second linear curve, starting at an AoA of 10°. Due to the linear stall behaviour, the lift coefficient is increasing and leads to massive errors in high AoA with an increasing tendency for increasing AoA. The XROTOR drag matches excellently in a narrow band around the minimum drag, but the error increases with the

Table 1 Source of 2D data base in different tools

	2D data base source	
	Source	Representation
JavaProp	JavaFoil	Discret polars
XROTOR	Arbitrary	Function
JBlade	XFOIL (XFLR)	Discret polars
RAALF	Arbitrary	Discret polars
PropCODE	XFOIL	Discret polars

Table 2 Reynolds number scaling coefficients [41]

Reynolds number	Reynolds number scaling exponent f
> 2.000.000	$-0.2 > f < -0.1$
200.000–800.000	$-1.5 > f < -0.5$
< 100.000	$-0.5 > f < -0.3$

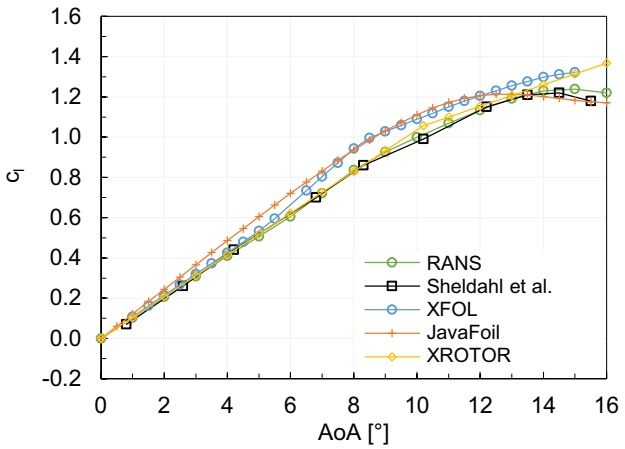

Fig. 2 NACA 0015 Airfoil cl-AoA polar at Re = 6.8E5

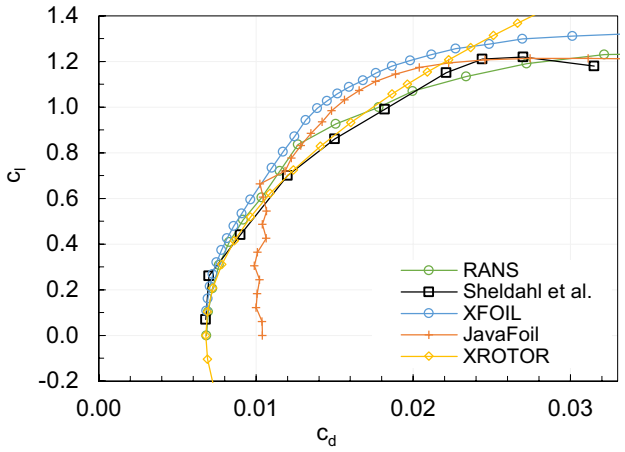

Fig. 3 NACA 0015 Airfoil cl-cd polar at Re = 6.8E5

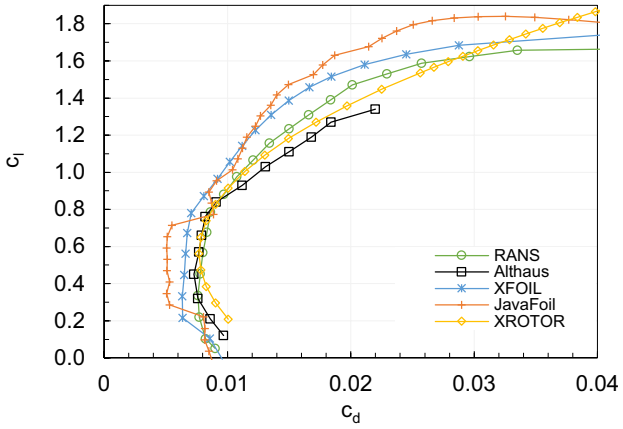

Fig. 5 SM 701 Airfoil cl-cd polar at Re = 1E6

lift coefficient. The error is diverging for high lift coefficients due to the parabolic modelling approach.

In the secondary case, JavaFoil is overpredicting the maximal lift by a Δc_l of 0.33 at 11°, equal to 20%, and has a higher lift slope (see Fig. 4). Concurrently, JavaFoil predicts a laminar dip (see Fig. 5). This laminar dip is less pronounced by XFOIL and not visible in the RANS simulation data and the experiment. The RANS simulation matches the experimental data best but overpredicts drag in the high lift region. Again this could result from imperfections in the experiment or wrong predicted positions of separation bubbles. Lift prediction of XFOIL and RANS matches experimental data with an accuracy of less than 5% error. RANS shows its strength in the pre-stall region by excellently matching experimental data but has some weaknesses in the drag prediction in the high lift region.

A close look at the experimentally measured lift curve shows a kink of the polar at approximately 0° AoA. This kink shows the drawbacks of the linear modelling approach of XROTOR, because the linear lift slope must be defined anyhow but is constant for the linear part of the curve, which leads to errors in the linear part (here for AoA below 0°). Again minor errors in the stall region are present but significant errors will occur in the post-stall region. The experimental drag polar shows a laminar dip, which the XROTOR approach cannot realise. This laminar dip results in a derivation from the experimental data at high lift coefficients. The parabolic polar approach results in a symmetric drag polar around the zero AoA lift coefficient of 0.59, leading to significant errors in low and negative lift regions.

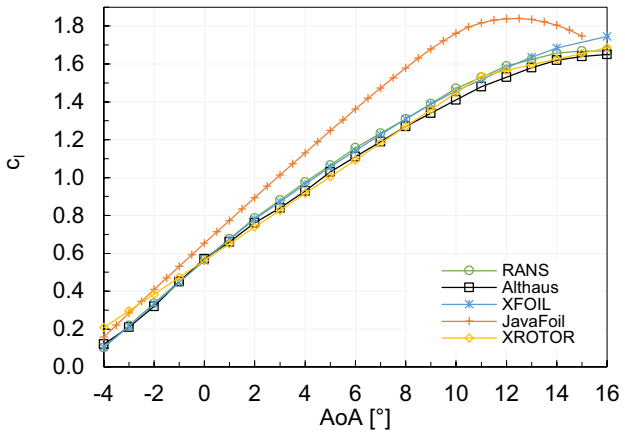

Fig. 4 SM 701 Airfoil cl-AoA polar at Re = 1E6

The RANS simulations match the wind tunnel test best. Accurate BET simulations need up to 20 blade sections and 20 polars, with 20 polar points for negative and positive AoA, each. The driving parameters for Mach number and Reynolds number effects are the rotational speed, the free stream velocity, and the temperature. Holding temperature and free stream velocity constant in static operations and calculating three different rotational speeds as presented in this publication required 1200 2D RANS simulations. Assuming that one polar point requires a computational time of 10 min, which will be incredibly fast; the airfoil data generation might require 67 h. Less time is necessary for one RANS MRF simulation of one operating point on a workstation (Sect. 2.2). Therefore, RANS simulations are not an adequate source for 2D aerodynamic data in BET simulations in an optimisation routine or early propeller design stages.

For this field of application, XFOIL should be selected as 2D aerodynamic data source. XFOIL predicts drag and lift with less derivation from the wind tunnel tests and calculates more consistent results than JavaFoil. The higher reliability is explained by a better match of trend and magnitude than JavaFoil. XROTOR matches the base configuration well, in this case, the experimental data, in the linear region for

airfoils without significant laminarity. However, significant errors occur in high AoA.

2.1.3 Investigated low-fidelity simulation tools

2.1.3.1 JavaProp JavaProp, developed by Hepperle [19], uses the procedure of Larrabee [54] and Adkins and Liebeck [55] in a graphical user interface (GUI) application. The application uses various input parameters for the design of the propeller for minimum induced loss operations derived by Betz and Prandtl [56]. To calculate the performance of existing propellers, JavaProp can be coupled with the 2D airfoil solver JavaFoil. The generated polar of JavaFoil have to be loaded into JavaProp to use them for propeller simulations [57]. The design approach bases on a blade element model coupled with a fixed wake LLT approach. This approach solves the LLT in a closed form and does not resolve the wake. However, the analysis approach is based on the work of Glauert [42]. Glauert uses the momentum approach to predict propeller performance, which also does not require resolving the wake. JavaProp slices the propeller into four airfoil sections and interpolates between these sections for the final thrust and torque.

2.1.3.2 XROTOR Drela has developed the tool XROTOR [48] for rotor aerodynamics, a derivation of Qprop for horizontal axial wind turbine simulations. XROTOR needs detailed design parameters along the propeller span as an input for calculating a propeller with an LLT method. The method requires a specific 2D airfoil polar format. The polars are transformed into a mathematical parabolic description using typical airfoil polar characteristics, e.g., minimal drag, zero-lift angle, maximum lift. The mathematical handling of 2D data coupled with a Fortran-based programming language allows computational efficient simulations. However, there is no direct connection or interface between XROTOR and XFOIL. XFOIL polars could be used as an input for XROTOR but must be transformed into the mathematical description.

XROTOR has four different induced velocity schemes incorporated; a nonlinear momentum formulation, a potential formulation according to Ref. [58], and a free vortex and fixed vortex wake LLT approach. In this publication, the potential formulation of the XROTOR standard scheme is selected, because the scheme is fast and robust. The potential formulation does not require resolving the wake, allowing fast turnaround times. The potential formulation is solved in a closed iterative procedure.

2.1.3.3 JBlade Another tool treating the open propeller aerodynamics is JBlade, an advanced GUI-based design tool [59]. JBlade is based on QBlade, an LLT optimisation procedure for horizontal axial wind turbine applications. JBlade uses 2D data from XFLR, a GUI-based development of XFOIL. Selectable post-stall and aspect ratio models adapt the 2D XFOIL data for high AoA propeller operations explained in Refs. [21, 60, 61]. The advantage over JavaFoil and XROTOR is the direct implementation of 2D data generation in the GUI without importing 2D data from other sources. However, a 2D aerodynamic data import from wind tunnel tests is not possible in this application.

In addition, a 3D representation of the propeller is generated during the design, and an export function for the generated propeller CAD is implemented. For appropriate use of JBlade, the propeller geometry has to be properly known with information about the twist, chord and airfoil distributions.

The aerodynamic model is based on the nonlinear momentum approach described in Eqs. 9–12 according to Ref. [26].

2.1.3.4 RAALF The RAALF [22] project is a Matlab propeller design and calculation environment developed by Bramesfeld and Ryerson University [62]. Different modelling approaches are realised to simulate propeller wing interactions, mainly with LLT and panel methods. The robust BET, coupled with nonlinear momentum theory, is used for comparison to the existing tools. Higher order LLT or panel methods are not used due to instabilities in the calculation procedures. The RAALF tool has opportunities to simulate cross-flow conditions but cannot design a propeller for minimum induced loss operations. Bramesfeld's research focus is on higher order potential flow solvers [22, 62–64].

2.1.3.5 PropCODE PropCODE—"Propeller comprehensive optimisation and design environment"—is an in-house Matlab propeller calculation procedure with a focus on aeroacoustic and aeroelastic of open propeller and ducted fans. The method is developed in cooperation with Helix Carbon GmbH, a carbon fibre propeller manufacturer. The method is used to develop a less noisy and lightweight propeller for urbane air mobility and general aviation. Lightweight propellers are required for high controllability in hover conditions. Due to the lightweight carbon structure, the mass inertia is reduced, which improves the system's response characteristics. A coupled optimisation and calculation scheme is developed to analyse the interactions between aeroacoustic and aeroelastic effects. Therefore, a validated aerodynamic calculation procedure must provide reliable input data for the acoustic and elastic simulation. The tools JavaProp, XROTOR, and JBlade, are partially a black box, where the users have no access to the source code. For acoustic and elastic simulations, the propeller's relevant flow phenomena must be simulated by the aerodynamic module. An in-house development could only provide this capability.

The PropCODE can use different induced velocity correction methods coupled with XFOIL for the 2D airfoil data. The 2D data can be adjusted with a sweep correction and a post-stall correction model to generate 3D aerodynamic data [61]. Compressibility and viscous effects are simulated with XFOIL. Different momentum equation models are realised for simulation of static, high-speed, and recuperation operation, e.g., [59, 65]. The baseline in this publication for the comparison with the other tools is a linear momentum theory. The approach is combined with the Prandtl tip loss correction procedure without post-stall and sweep correction models. The baseline is further compared against a nonlinear momentum approach and an LLT correction method.

The linear momentum approach smears the axial induced velocity over the propeller disk. A constant induced velocity is calculated according to the following equation in the propeller disk, derived by the general momentum theory [34]:

$$w_{\mathrm{a}} = -\frac{v_{\infty}}{2} \pm \sqrt{\left(\frac{v_{\infty}}{2}\right)^2 + \frac{T}{2 \cdot \rho \cdot A_{\mathrm{Prop}}}}. \tag{13}$$

The nonlinear momentum approach discretises the propeller disk by ring elements and applies the momentum approach per element. Axial and tangential induced velocities on each ring element are calculated according to the following equations [31, 66]. This approach predicts a nonlinear induced velocity distribution, known as the nonlinear momentum approach:

$$w_{\mathrm{a}} = v_{\infty} \cdot a_{\mathrm{a}}, \tag{14}$$

$$a_{\mathrm{a}} = \frac{\left(1 + a_{\mathrm{a}}\right) \cdot \sigma \cdot \left[c_{\mathrm{l}_{\alpha}} \cos(\phi) - c_{\mathrm{d}_{\alpha}} \sin(\phi)\right]}{4 \sin^2(\phi)}, \tag{15}$$

$$w_{\mathrm{t}} = u \cdot a_{\mathrm{t}}, \tag{16}$$

$$a_{\mathrm{t}} = \frac{\left(1 + a_{\mathrm{t}}\right) \cdot \sigma \cdot \left[c_{\mathrm{l}_{\alpha}} \sin(\phi) + c_{\mathrm{d}_{\alpha}} \cos(\phi)\right]}{4 \sin^2(\phi)} \cdot \frac{v_{\infty}}{u}, \tag{17}$$

where ϕ is the so-called helix angle, spanned between relative velocity and plane of rotation. σ is the solidity of the blade, a measure for the chord length of a blade section to the belonging circumference.

The LLT correction model calculates axial, tangential, and radial induced velocities using potential theory. According to Ref. [67], the procedure calculates the bounded circulation on the blade and the induced velocities. The linear and nonlinear momentum approaches are time-independent simulation techniques, while the LLT procedure is resolved in the time domain in this work. No ground effect is taken into account in hover conditions.

A semi-prescribed wake model is used for the LLT procedure, which prescribes the wake form by the RPM but calculates the advance ratio with the time-dependent inflow velocity. In comparison, a fully prescribed wake model uses the flight velocity for the advance ratio calculation and, therefore, for determining the wake helix shape. The fully prescribed wake model is worse in static conditions, because the shedding circulation lines build up behind the propeller. This build-up increases the induced velocity and, therefore, decreases thrust and power prediction.

The basic equation for coupling potential theory with resulting forces is stated in Eq. 18. Further information about the calculation scheme could be obtained from Ref. [67]:

$$\Gamma = \frac{1}{2} \cdot c_{\mathrm{l}_{\alpha}} \cdot C_{\mathrm{Chord}} \cdot w, \tag{18}$$

where Γ is the circulation of an airfoil, which describes the streamline deflection.

An iterative procedure determines the final induced velocity and, therefore, the final effective AoA and propeller performance. The iterative procedure uses the different induced velocity calculation schemes but the same correction methods and force calculation functions. The initial induced velocity is zero and iteratively calculated until the resulting thrust remains constant.

PropCODE uses the manufacturing geometry as an input, slices it into airfoils, and determines chord and twist distributions. This information is automatically used to calculate 2D aerodynamic data.

2.2 High-fidelity propeller simulation methods

High-fidelity RANS simulations are performed with the commercial software StarCCM+. StarCCM+ provides different simulation techniques for propeller simulations, while in this paper, two different procedures are used. Virtual disk approaches could not be used for validation purposes, because the propeller's surface is replaced by source terms that depend on the unknown forces. Only surface representing simulation techniques can be used for validation purposes. The techniques are a rigid body motion, a moving reference frame approach, a sliding mesh approach, and a morphing mesh approach. The latter is intended for non-rigid motion [68].

2.2.1 Moving reference frame

The moving reference frame (MRF) technique requires a mesh attached to the propeller in the flow domain, with an independently rotating coordinate system. Information of the separate moving reference frame mesh is transported cell by cell over the mesh interface between the rotational and steady regions. A steady simulation of the rotating

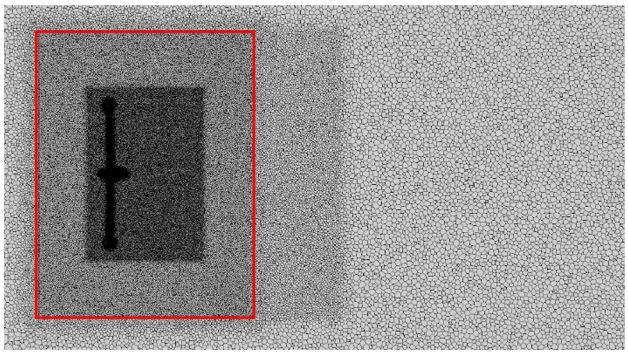

Fig. 6 MRF mesh side view

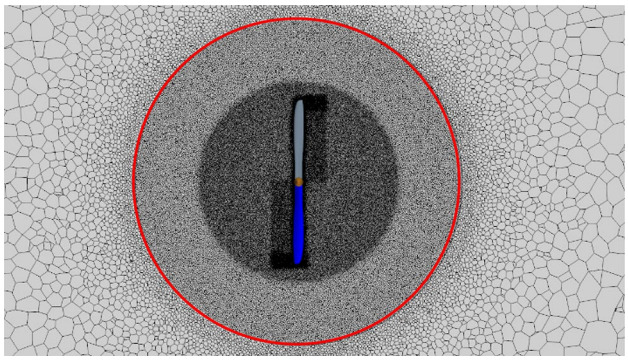

Fig. 8 MRF mesh front view

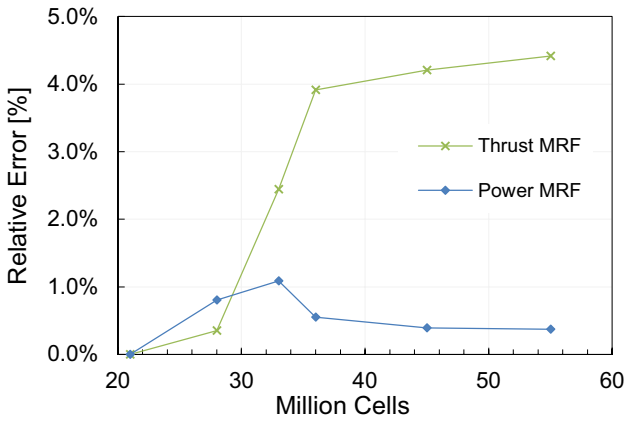

Fig. 7 Mesh independence study H25F: static test case: MRF

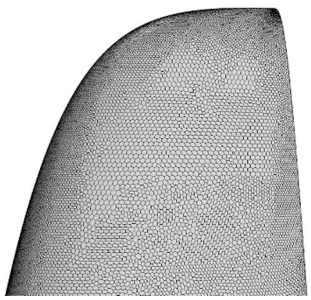

Fig. 9 Propeller tip surface resolution

part reduces the calculation effort but does not resolve the unsteady effects. This procedure allows to perform a steady-state simulation and thus reduces the computational effort significantly. A more comprehensive review of RANS and URANS propeller simulations is provided by Ref. [69]. The helical slipstream velocity information is smeared in the static part of the mesh domain, which is why this simulation technique cannot model rotor–stator or rotor–wing interaction.

The simulation domain is discretised with 36 million polyhedral cells. Local refinements of the poly mesh are necessary at the propeller tips because of tip circulation and at the propeller root because of flow separation. Further refinements are placed in the wake. The cell size in the wake is gradually increased to reduce the calculation effort. The red rectangular shape in Fig. 6 is the cylindrical moving reference frame. During the mesh independence study, the wake resolution is reduced to a minimum (presented in Fig. 7). 36 million polyhedral cells is a balance between computational effort and simulation accuracy. An efficient simulation with 36 million cells is possible, because the relative change between 36 and 53 million cells is less than 0.3% in thrust and power consumption prediction. In comparison, the computational effort is doubled by an increase from 36 to 53 million polyhedral cells. One iteration with 36 million polyhedral cells needs 29 s on 30 AMD EPYC 7742 CPU cores, while 53 million cells need 32 s on 60 AMD EPYC 7742 CPU cores.

In Fig. 8, the MRF mesh domain is presented in the front view. The wake refinement, as well as the tip refinement, are visible. In addition, the already mentioned MRF cylinder can be seen.

The boundary layer is modelled with a low $y+$ approach and 25 prism layers. About 75 cells are placed in chord direction with additional refinements at the leading and trailing edge (see Fig. 9). The number of surface cells determines the total number of cells if a smooth transition from fine to coarser meshes is desired (see Fig. 10).

The flow field is solved using a coupled flow solver with the SST (Menter) k-ω turbulence model [48]. For solving the Navier–Stokes equations, an upwind scheme for the convective fluxes and a central differences scheme for the viscous fluxes are used. Both schemes are second-order accurate. In the turbulence model, the quadratic constitutive relaxation scheme is used [70]. The freestream turbulence viscosity ratio is set to 10 in combination with a "controlled decay model" [71].

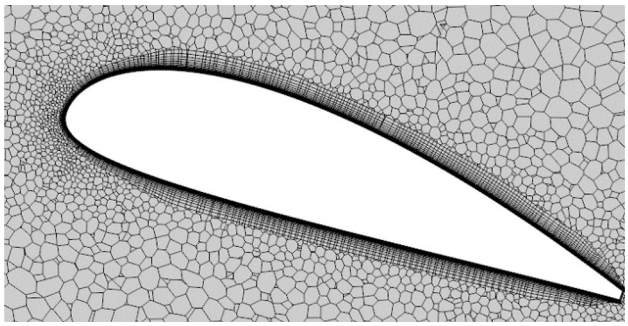

Fig. 10 Prism layer mesh resolution

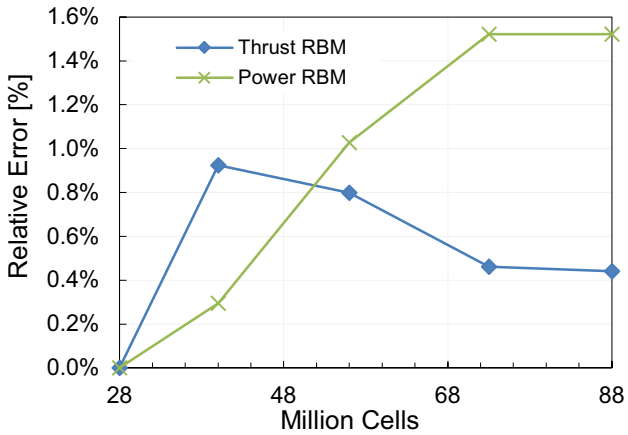

Fig. 11 Mesh independence study H25F: static test case: RBM

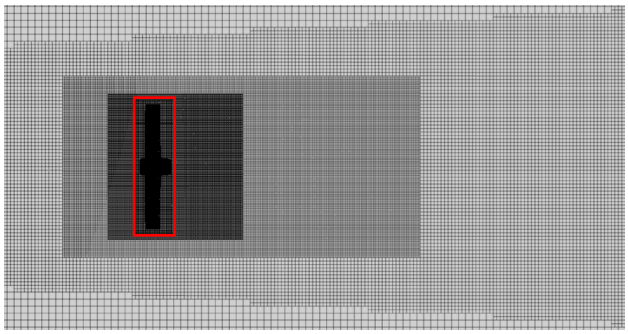

Fig. 12 RBM mesh side view

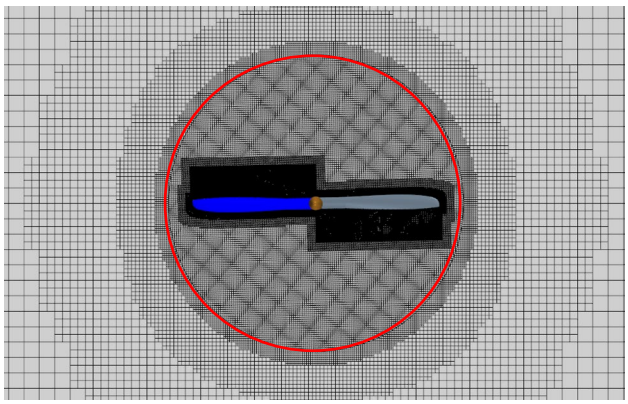

Fig. 13 RBM mesh front view

The total elapsed time consumption for one operating point with an MRF simulation is approximately 12 h. The simulations are performed with 30 AMD EPYC 7742 CPU cores.

2.2.2 Rigid body motion

The sliding mesh technique is used to create a real motion of a mesh region. As for the multi-reference frame technique, a part of the flow domain around the propeller is separated and rotates. For each time step, a new interface section has to be calculated.

The physical model and the mesh resolution is equivalent to the MRF simulation except for the change to an unsteady simulation. The mesh independence study (Fig. 11) shows that RBM methods could handle smaller moving mesh domains than MRF simulations (see Figs. 12 and 13). The moving domain is marked with the red rectangular shape in Fig. 13. The smaller domain is explained by the information loss in MRF simulations, which are transported by the RBM simulations over the domain interfaces. Because of memory requirements during the mesh independence study, the RBM simulation is switched from poly to the trimmed mesh. 52 million trimmed cells are used. The trimmed mesh requires approximately half of the memory during calculation. Therefore, much more cells can be simulated. The surface representation, prism layer settings, and the local refinements are equivalent to the MRF simulation.

The loss of information in the MRF simulation can be seen in Fig. 14, where the transition from static to rotating part is located in the middle of the figure. In the rotating part upstream, the shedding helix vortex is represented by the increased velocities, while in the static part downstream, the vortex cores are smeared and not visible.

Compared to the MRF simulation, the RBM simulation is a time-dependent simulation. Therefore, this procedure can be used for rotor–stator and rotor–wing interactions. Figure 15 presents the differences to the MRF approach, where the shedding vortices presented as high-velocity cores are visible in the whole flow domain.

For visualisation purposes, the velocity scenes (Figs. 14, 15) are clipped between 5 and 30 m/s. All velocities above or below are coloured in blue or red.

A converged solution in the RBM approach is achieved after 2–3 rotations with a movement of less than one degree

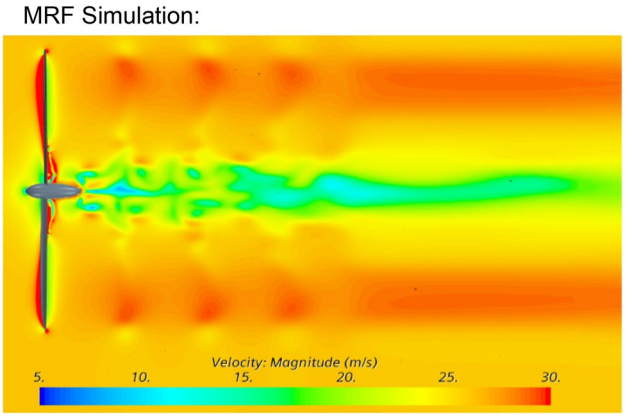

Fig. 14 Moving reference frame simulation H25F diameter 1.25 m 2 blades

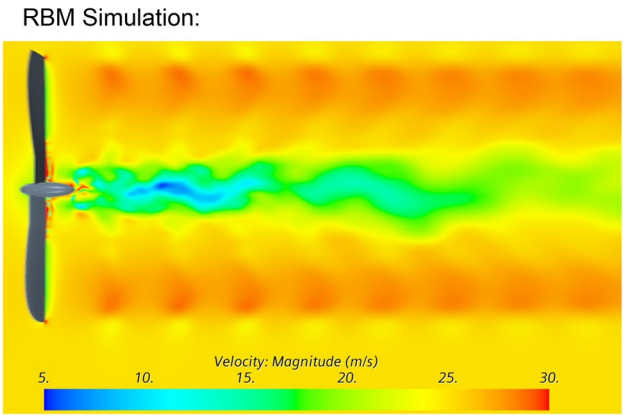

Fig. 15 Rigid body motion simulation H25F diameter 1.25 m 2 blades

per time step. One degree per time step results in time steps for the rotation speed of 2500 RPM of 6.6e−7 s. Another 2–3 rotations have to be used to calculate the integrated thrust and power consumption. Figure 13 is taken after six rotations.

The total elapsed time for an MRF simulation is less than 12 h. In comparison, one operating point with the RBM simulation approach requires 96–168 h, depending on the operation point. Therefore, if MRF and RBM results are comparable and MRF delivers sufficient accurate results, MRF simulations should be selected for open propeller simulation.

3 Propeller data

Two propellers of the propeller manufacturer Helix-Carbon GmbH are simulated for validation purposes. The propellers are shown in Fig. 14.

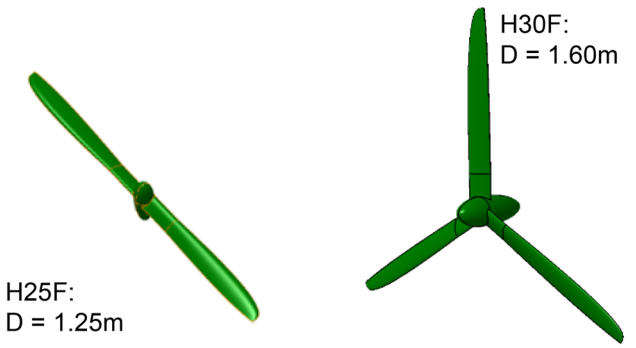

Fig. 16 H25F (left) and H30F (right) CAD model

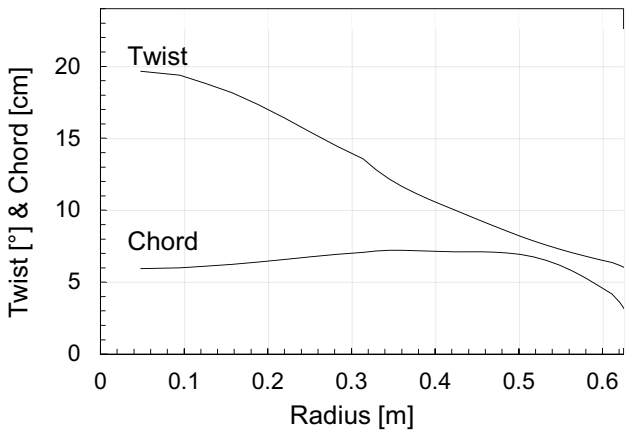

Fig. 17 Twist and chord distribution of H25F, diameter 1.25 m, two-bladed propeller

The first propeller on the left-hand side of Fig. 16 has two blades with a diameter of 1.25 m. The chord and twist distribution is presented in Fig. 17. The normalised pitch at 75% radius is 11°. The propeller name "H25F 1.25 m R-Z-06-2" gives information about the stiffness class (H25), fixed or variable pitch (*F*) the diameter, the turning direction (left/right), the configuration [pusher (*S*) or puller (*Z*)], the root additional inclination angle in degree (6° at the tip) and the number of blades (2). The propeller is mainly used in paraglider applications.

Helix–Carbon GmbH had provided additional information about thrust and power consumption. The propeller is tested on a static test bench driven by an electric motor. Thrust and torque are directly measured at the driving shaft for different rotational speeds. Figure 18 shows the static test bench results of the H25F propeller.

The second propeller, “H30F 1.60 m R-Z-05-3”, has three blades, a diameter of 1.6 m, a normalised pitch of 9° at 75% radius, and following twist and chord distribution (see Fig. 19). The application spectrum of the H30F propeller

is ultra-light and small general aviation aircraft. Static test bench data are presented below (see Fig. 20).

4 Result evaluation

The different BETs are compared with the static test bench data provided by Helix–Carbon GmbH—in case one with two different high-fidelity RANS simulations (MRF and RBM), and in case two with MRF simulations. The RANS simulations are performed with a generic hub to avoid flow separation at the propeller's root. The highest available simulation is used as reference data for advance ratios above zero, because no wind tunnel tests exist. Therefore, the RANS simulations are validated in the static case with test data and can be used as a reference for higher advance ratios. Thrust and power consumption curves for the propeller are plotted in the following figures.

The performance curves are calculated with different velocity step sizes. JavaProp performs an automatic stepping. The curves with JBlade, XROTOR, RAALF, and PropCODE have velocity steps of 1 m/s. The MRF simulations are calculated with fixed advance ratio steps of 0.05, except in ultra-low advance ratios, where a step size of 0.025 is selected. The smallest advance ratio in MRF simulation is 0.025, because lower advance ratios cause flow instabilities that cannot be resolved with MRF. Most BET cannot calculate zero flight velocity because of numerical instabilities. In these cases, the free stream velocity is set to 0.1 m/s instead of 0 m/s, resulting in an advance ratio error of 0.0032.

Case one treats the H25F 1.25 m two-bladed propeller at an RPM of 2500, while case two is about the three-bladed propeller at an RPM of 2000. At first, the comparison for case one is presented. After comparing the simulation tools in Sects. 4.1 and 4.2, the induced velocity schemes are analysed in Sect. 4.3. Finally, the influence of changes in lift and drag coefficient is analysed in Sect. 4.4.

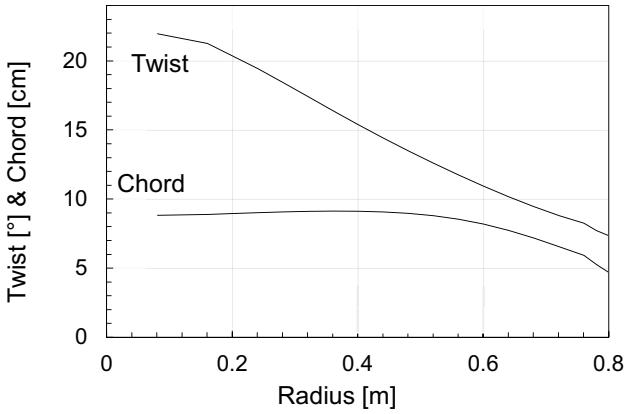

Fig. 19 Twist and chord distribution of H30F, diameter 1.60 m, three-bladed propeller

4.1 Case 1: H25F 1.25 m two-bladed propeller

The simulation results for case one are compared in the following five diagrams. Introduced BET tools, the MRF and the RBM RANS simulations are compared against static data in Figs. 21 and 22 and Tables 3 and 4.

First, comparison of the static thrust to the simulation results of the RANS approaches shows that RMB and MRF simulations match experimental data with less than 8% error with regard to the test data. The static RBM thrust is slightly below the MRF thrust, but the difference between RBM and MRF is below 5%, acceptable for less than 10% of the calculation time. Therefore, the RANS prediction can be used for further comparison. Both methods underpredict thrust, which might result from changed effluent conditions between experiment and RANS simulation. Similar behaviour is observed in power consumption. However, power consumption for the higher rotational speeds matches within 4%, leading to a slight

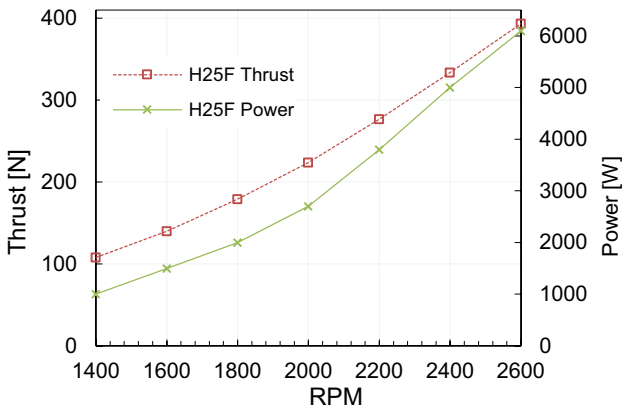

Fig. 18 Static test case H25F, Diameter 1.25 m, two blades

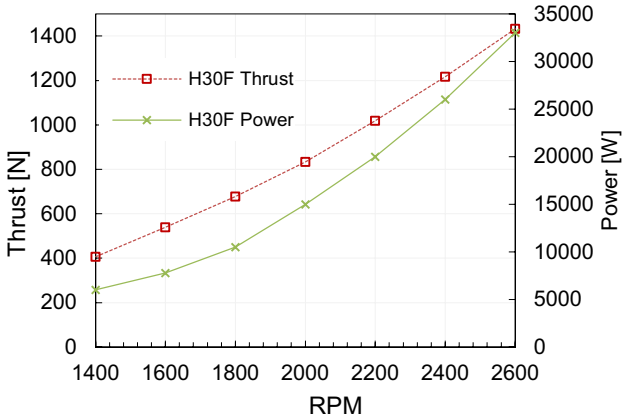

Fig. 20 Static test case H30F, diameter 1.60 m, three blades

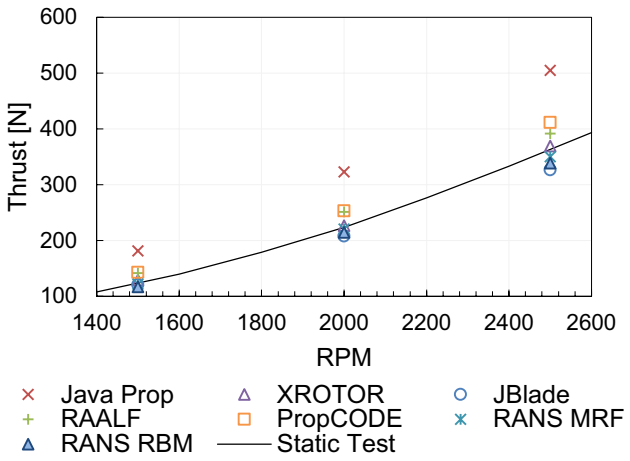

Fig. 21 H25F: static thrust comparison

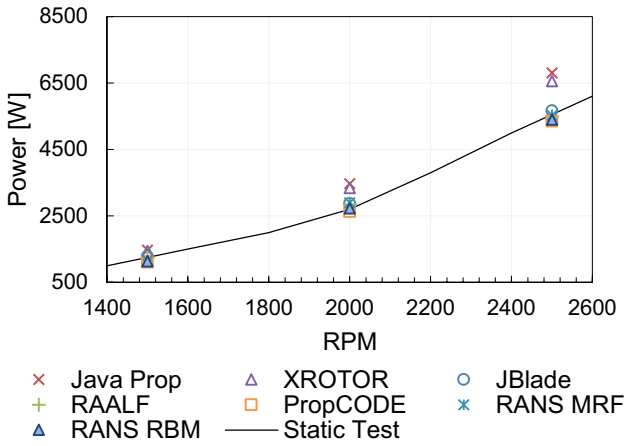

Fig. 22 H25F: static power consumption comparison

overprediction of the MRF simulation of 2%, while the RBM simulation still underpredicts power consumption.

JavaProp is overpredicting the static thrust by about 44%. XROTOR and JBlade are in a 10% relative error range, while the PropCODE and the RAALF project have relative errors of below 18% to the MRF simulation. The mismatch of JavaProp is due to the airfoil lift prediction of JavaFoil with significant errors of about 20%. The worse lift prediction directly results in an overprediction of thrust, as stated in Eq. 3.

Different behaviour is observed for the static power consumption comparison, where XROTOR overpredicts power consumption by 25%. Worse is only JavaProp with a maximal overprediction of 27% error compared to the MRF approach. The relative error of the power prediction of the tools RAALF and JBlade are below 11%. The PropCODE shows a decreasing relative error for higher loading conditions, respectively, higher RPM. The mismatching of XROTOR is due to the airfoil drag modelling, which has significant errors at high lift coefficients equal to low advance ratios. As for the thrust prediction, the error of JavaProp results from the error of JavaFoil, as stated in Eq. 4.

The following table summarises the relative errors of the high fidelity RANS simulation compared to the static test case. As shown in Table 3, the relative errors of the RBM approach are in a range of 10% compared to experimental data. The error could be explained by measurement equipment, the propeller drive, ground effects, or the motor control unit, while the RANS simulation contains just a generic hub and no additional equipment. The RBM approach is used as a reference for further comparison of the H25F propeller, because it simulates the same undisturbed propeller, as analysed in the BET simulations. The difference between MRF and RBM compared to the static test case is similar. Therefore, the MRF approach can be used for further comparison between BET and RANS as reference.

Table 4 summarises the relative errors of the BET approach compared to the RANS MRF approach in static operations. The RANS MRF approach is used as the baseline for further comparison.

The comparison between the high-fidelity RANS simulation and the BET methods at higher advance ratios shows that JBlade behaves incorrectly up to a certain advance ratio (Figs. 23, 24, 25). Detailed analysis shows that the post-stall modelling used in JBlade leads to this incorrect behaviour. The post-stall behaviour can adapt the 2D airfoil polars predicted with XFOIL to the post-stall region required for deep-stall. The post-stall behaviour is combined with a three-dimensional correction according to Ref. [61].

JavaProp is permanently overpredicting thrust and power consumption, which results from the 2D polars. XROTOR again shows the best conformity with the high-fidelity thrust

Table 3 H25F relative error of RBM RANS simulation compared to static test data

RPM (1/min)	Thrust			Power		
	1500	2000	2500	1500	2000	2500
Relative error of RANS against static tests results						
RANS MRF	– 4%	– 3%	– 4%	– 8%	2%	1%
RANS RBM	– 8%	– 6%	– 7%	– 9%	– 4%	– 2%
Static test	127 N	228 N	363 N	1250 W	2850 W	5500 W

Table 4 H25F: relative error compared to RBM RANS simulation

RPM (1/min)	Thrust			Power		
	1500	2000	2500	1500	2000	2500
Relative error of BEM against static tests results						
JavaProp	49%	47%	44%	27%	20%	23%
XROTOR	6%	3%	6%	25%	15%	19%
Jblade	− 1%	− 6%	− 7%	11%	− 1%	2%
RAALF	16%	14%	12%	7%	− 2%	− 1%
PropCODE	17%	15%	18%	− 4%	− 9%	− 3%
RANS MRF	122 N	220 N	350 N	1154 W	2901 W	5530 W

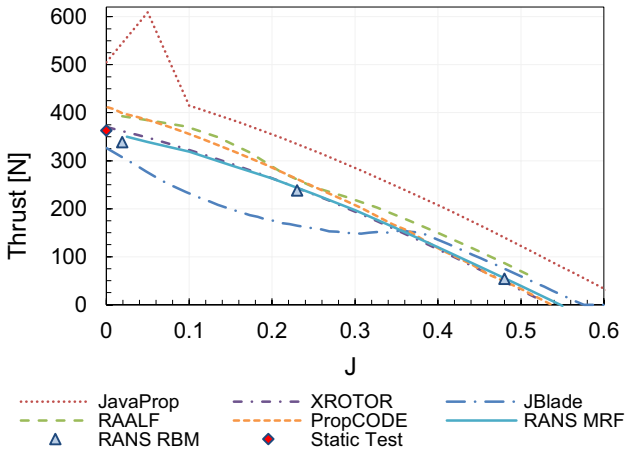

Fig. 23 H25F: thrust over advance ratio at RPM 2500

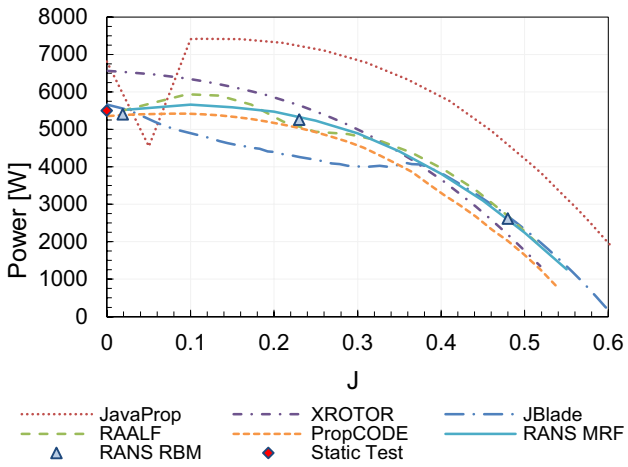

Fig. 24 H25F: power over advance ratio at RPM 2500

simulation but differs in the power consumption prediction in magnitude and trend. This phenomenon is due to the drag coefficient's parabola airfoil polar fitting procedure, creating errors in low and high AoA conditions. Still, it is fast and stable in moderate advance ratio conditions. All the other tools directly work with polar points and use interpolation or

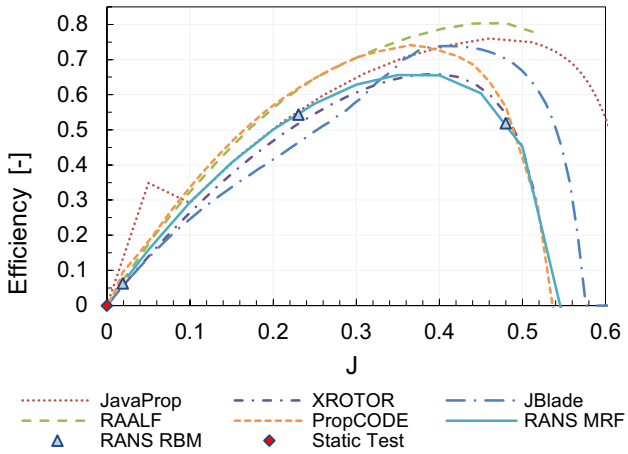

Fig. 25 H25F: efficiency over advance ratio at RPM 2500

fitting functions to represent the 2D aerodynamic data. PropCODE and RAALF show minor relative errors to the high-fidelity data of around 5–10%. The MRF simulation and the RBM simulation match thrust and power consumption for high advance ratios, and therefore, the efficiency curves are also corresponding. The perfect matching of MRF and RBM allows using the faster MRF approach for further validation.

Thrust and power consumption errors in the efficiency curves (Fig. 25) are cumulated and enhanced in high advance ratio conditions with the inflow velocity. The ratio of thrust to power is combined with the free stream velocity. Low free stream velocities reduce absolute errors of thrust and power in the efficiency curves. Therefore, the efficiencies should only be evaluated for high advance ratios.

JavaProp shows a good agreement to the high-fidelity data after overcoming the non-physical bump above advance rations of 0.1, but this is an artificial accuracy and not an indication for high accuracy due to the error accumulation. However, most BET methods do not simulate maximal efficiency correctly except for XROTOR, which matches the MRF efficiency curve in a wide range. The matching of XROTOR's efficiency predictions results from the excellent match in thrust prediction and the error in power consumption trend. The error in power consumption is high at low J

conditions, so these errors are accumulated with the flight velocity and are, therefore, less important. The changed slope leads to relatively small relative errors for higher advance rations resulting in a good match of efficiency (Fig. 25). The PropCODE simulates maximum efficiency at the correct advance ratio but overestimates it by 15%. However, the results of PropCODE follow the trend of the RANS simulation.

RBM and MRF's differences are neglectable in integrated thrust and power consumption at the critical design points, low advance ratios and high advance ratios. The propeller's flow conditions are relaxed in moderate advance ratios, and these simulations are not critical for validation purposes. The relative error between MRF and RBM simulation is less than 5.1% at all advance ratios. The steady MRF simulation has stability issues in shallow advance ratio conditions. These are caused by flow separation effects at the root of the propeller, which a steady simulation approach cannot capture. The flow separation effects propagate along the propeller span to the tip when the inflow velocity decreases further. RBM is always an unsteady simulation, so this simulation technique is suitable for low advance ratio conditions. For stability issues, it is possible to switch the MRF simulation to an unsteady simulation, which is still much faster than the RBM approach, because higher time steps can be used. The time-step in the RBM approach is adjusted to resolve the rotation. The time-step in the unsteady MRF approach is adjusted to the stall region, allowing higher time-steps as required for the RBM simulations.

MRF requires approximately 10% of the CPU time of RBM simulation. However, the simulation results differ only slightly. Therefore, the MRF simulation results are used as reference for further comparison.

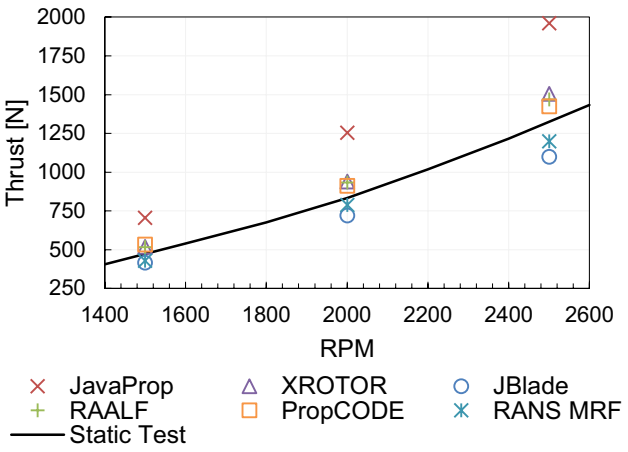

Fig. 26 H30F: static thrust comparison

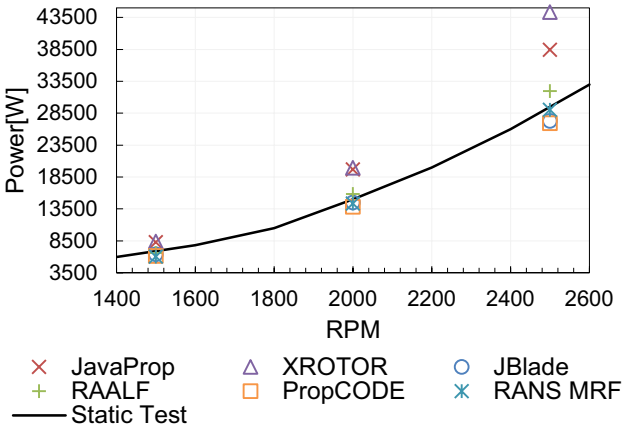

Fig. 27 H30F: static power consumption comparison

4.2 Case 2: H30F 1.60 m three-bladed propeller

The RBM simulation is not performed in case two, because RBM shows no significant difference to the MRF simulation but requires ten times the computing time. The efficiency is not further analysed because of the explained error accumulation effect.

As for case one, static results are shown in Figs. 26 and 27 and Tables 5 and 6. The higher advance ratio results are shown in Figs. 28 and 29.

The comparison of the static case shows a good match between MFR and static case with relative errors of below 10%, again. Compared to case one, the relative errors are slightly higher, resulting in a stronger underprediction of the experimental data. However, RANS MRF can be used as a reference for further validation.

As in the first case, JavaProp is completely overpredicting thrust and power for the same reason as in case one. The static power prediction of the PropCODE and JBlade compared to the MRF simulation is matching within 7% relative error. Slightly worse is RAALF, with a relative error of 10%. The table of relative errors (Table 6) shows similar errors for all simulation tools compared with Table 4. However, the relative error slightly increases, because RANS has a greater derivation in static thrust compared to the test data.

In high advance ratio conditions, XROTOR shows a worse thrust estimation behaviour compared to the MRF simulation. Concluding, power consumption is increased due to an increased thrust prediction. The matching procedure of 2D data might be a reason for the worse matching. PropCODE predicts most accurate thrust and power consumption for increased advance ratios. JBlade, JavaProp and RAALF perform similar to case one.

Finally, the most accurate and consistent static performance simulation results for the static test case are performed with RANS simulation. Therefore, the RANS simulation can be used as a reference baseline to evaluate the low-order BET methods. In addition, the MRF simulation is

Table 5 H30F: relative error of RBM RANS simulation compared to static test data

RPM (1/min)	Thrust			Power		
	1500	2000	2500	1500	2000	2500
Relative error of RANS MRF against static test data						
RANS MRF	− 8%	− 6%	− 9%	− 10%	− 4%	− 2%
Static Test	468 N	839 N	1315 N	6651 W	15000 W	29500 W

Table 6 H30F: relative error compared to RBM RANS simulation

RPM (1/min)	Thrust			Power		
	1500	2000	2500	1500	2000	2500
Relative error of BEM against RANS MRF simulation						
JavaProp	64%	59%	63%	38%	37%	32%
XROTOR	21%	19%	25%	40%	39%	53%
Jblade	− 3%	− 9%	− 8%	6%	1%	− 6%
RAALF	20%	18%	22%	10%	10%	10%
PropCODE	24%	16%	19%	2%	− 4%	− 7%
RANS MRF	430 N	789 N	1200 N	6011 W	14358 W	29048 W

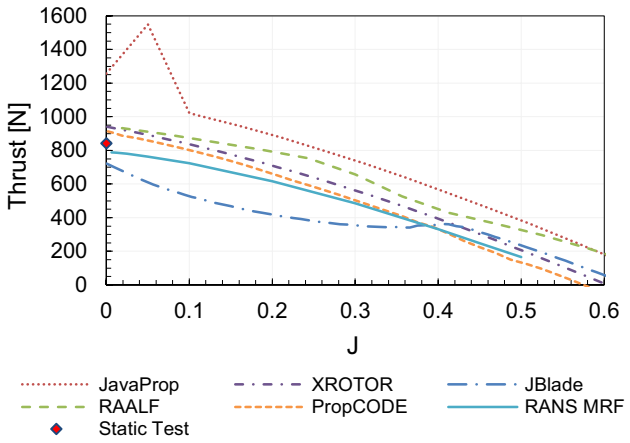

Fig. 28 H30F: thrust over advance ratio at RPM 2000

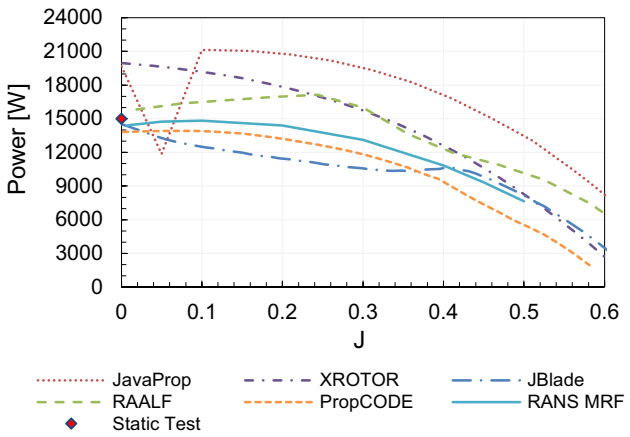

Fig. 29 H30F: power over advance ratio at RPM 2000

qualified for higher advance ratios with the RBM simulation. RBM simulations have no information loss in the wake due to the simulation approach, why they should be more accurate than the MRF simulation. Differences between MRF and experiment could result from measurement equipment, the drive, ground effects, and installation effects, which, for simplicity and convergence, are not simulated in the RANS simulations.

PropCODE is reproducible, underpredicting the power consumption and overpredicting the thrust. XROTOR is due to the 2D polar representation being more sensitive to input variations and has weaknesses in the power consumption predictions due to the parabolic fitting. JavaProp and JBlade do not sufficiently predict thrust and power consumption because of the non-physical behaviour at low advance ratios.

4.3 Induced velocity calculation scheme comparison in PropCODE

The differences in the presented simulation procedures result from different induced velocity calculation schemes, different correction methods, and different 2D data processing (as already described in Table 1). Three different schemes are implemented in PropCODE to analyse the effect of different induced velocity calculation schemes.

This subchapter shows the influence of the different induced velocity calculation schemes using the same environment and, therefore, the same data processing. Therefore, the influence of the different induced velocities can be evaluated. The used schemes are the linear momentum theory, the nonlinear momentum theory, and a semi-prescribed, wake resolving LLT approach. The LLT procedure with a fixed

wake is not implemented, because it cannot simulate low advance ratio conditions by nature.

The previously shown PropCODE results were computed with the most straightforward calculation scheme, the linear momentum theory. The simulation results are again compared against the MRF simulation. JavaProp uses the closed-form LLT formulation for the design, but for the performance calculation, the nonlinear Glauert formulation [42]. The XROTOR analysis is performed with the closed-form LLT formulation without any wake modelling (Table 7).

The comparison in Figs. 30 and 31 shows that the nonlinear momentum approach performs slightly better than the linear approach in low advance ratio conditions. Thrust and power prediction is closer to the RANS performance prediction. The slope of the nonlinear thrust calculation is slightly lower than the linear approach, which results in slightly worse matching between RANS and the nonlinear approach in higher advance ratio conditions. On the other hand, power is slightly higher in low advance ratio conditions and similar to the linear approach in higher advance ratio conditions. Therefore, the nonlinear approach slightly improves the calculation procedure, while the computational effort just increases slightly.

The LLT procedure with a semi-prescribed wake model predicts reduced thrust and, consequently, power compared to the linear and nonlinear approaches. However, the LLT procedure requires 30 times more CPU time, because the wake have to be resolved for the calculation scheme, which is not required in the momentum approach (momentum approach: 30 s for one performance curve with up to 30 points LLT approach: 15 min for one performance curve with up to 30 points). On the other hand, the method resolves the rotation of the blades in the time-domain, which can be useful for aeroelastic and aeroacoustic simulation.

Additional plots of the H25F propeller for the rotational speed of 1500 RPM are attached in the appendix. The three-bladed H30F propeller plots are shown in the Appendix for the rotational speed of 2500 RPM. The results of the H30F propeller shows the same behaviour for the different calculation schemes.

To better understand the differences between the simulation approaches, it is necessary to know that a propeller

Table 7 Induced velocity calculation scheme of the different simulation tools

	Induced velocity calculation scheme
JavaProp	Nonlinear momentum theory
XROTOR	Closed-form LLT formulation
JBlade	Nonlinear momentum theory
RAALF	Linear momentum theory
PropCODE	Linear momentum theory

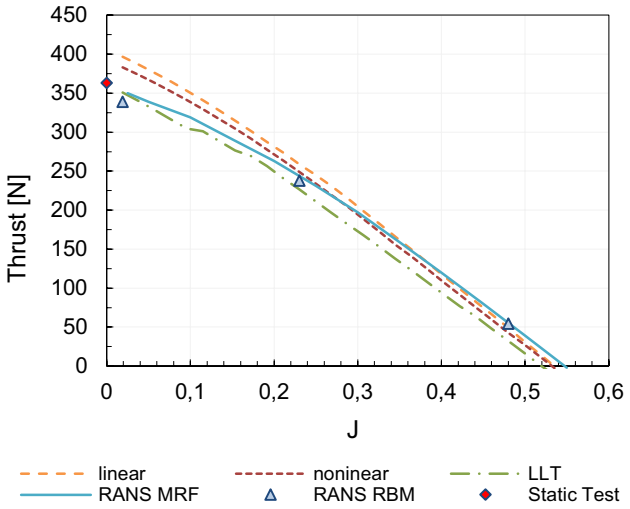

Fig. 30 H25F: thrust over advance ratio at RPM 2500: PropCODE comparison

creates the most thrust at the portion between approximately 70% and 95% relative radius (here: 0.4 m and 0.6 m). Aerodynamic forces increase quadratically with increasing rotational velocity (see Eqs. 2 and 3). Therefore, the inner portion of the propeller is less critical for the overall thrust. At the propeller tip above 95% radius, the tip vortex reduces the downwash and, therefore, lift by a vortex-induced upwash and finally reduces the thrust.

The improvement of the nonlinear model over the linear momentum model was expected due to the redistribution of velocities. The induced velocity at the propeller blade's outer radius is higher when applying the nonlinear momentum theory, while the induced velocity is reduced at the inner radius. The LLT procedure has compared to

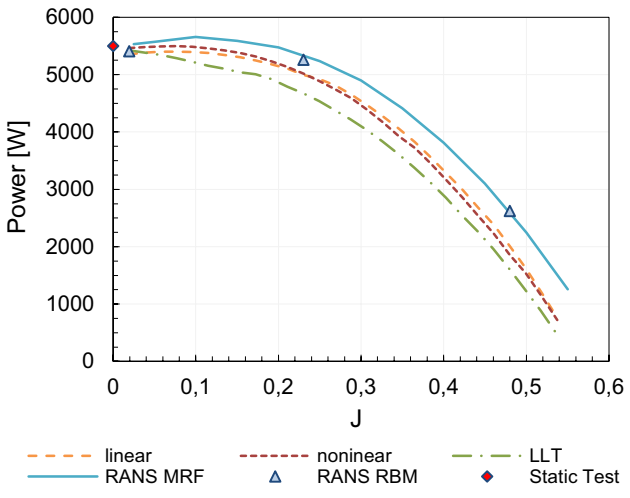

Fig. 31 H25F: power over advance ratio at RPM 2500: PropCODE comparison

the nonlinear momentum method a more complex induced velocity distribution. The maximum induced velocity is again increased compared to the nonlinear procedure (see Fig. 32). The increase of the induced velocities at the outer radius results in a reduced effective AoA. Therefore, lift and drag reduce slightly of the sections, and finally, results in a thrust reduction. However, the reduced effective AoA rotates the lift and drag vector and slightly increases the torque and power consumption. These effects are less pronounced in high advance ratio conditions, since the induced velocity is generally reduced for a fixed-pitch propeller. Furthermore, the flight velocity is higher, resulting in smaller changes due to the induced velocity.

4.4 Influence of 2D aerodynamic data variation in PropCODE

Finally, the influence of the 2D airfoil polars on overall thrust and power consumption is analysed. Lift and drag coefficients are artificially affected and increased by 10% separately and 10% together compared to the calculated XFOIL data. In addition, the drag is set to zero for evaluating the influence of inviscid simulations. PropCODE uses 2D XFOIL data which can be manipulated to analyse the need for high accuracy input data.

The analysis is performed with the H25F propeller and the linear momentum scheme. The analysis in Fig. 33 shows that the thrust calculation is mainly influenced by c_l. Changes in c_d has only a slight influence of the calculated thrust, which is straightforward, because c_d is two orders smaller and depends on the sinus (Eq. 3). Figure 33 depicts that a change of 10% c_l also results in a relative error in thrust prediction of 10%. Both coefficients influence the power consumption (Fig. 34), but a c_l increase has a stronger impact to the power consumption as a c_d increase. 10% c_l increase results in 7% relative error in the power consumption, while a 10% c_d increase results in only 3% relative error. Without drag, thrust is not affected, as concluded in Ref. [72]. However, the power consumption is significantly decreased, which is why accurate drag coefficients are required.

The study shows, that it is more important to have accurate c_l data than c_d, because c_l has a significant impact on the thrust prediction and power prediction, while c_d has only an impact on the power prediction. Furthermore, Figs. 2 and 4, presents the importance of having an accurate twist distribution of the propeller. One degree in the airfoil polars is in the linear region approximately a Δc_l of 0.1 which has an significant effect to the thrust and power consumption prediction. Evaluating the XROTOR approach, we get major errors in the high lift region, because the linear lift

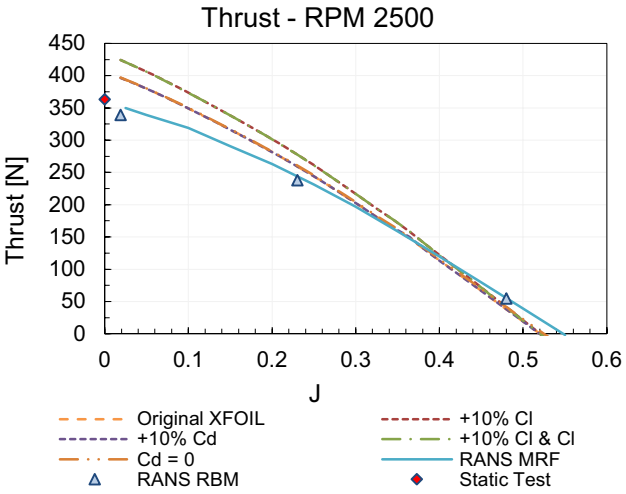

Fig. 33 H25F: influence of 2D data to thrust change

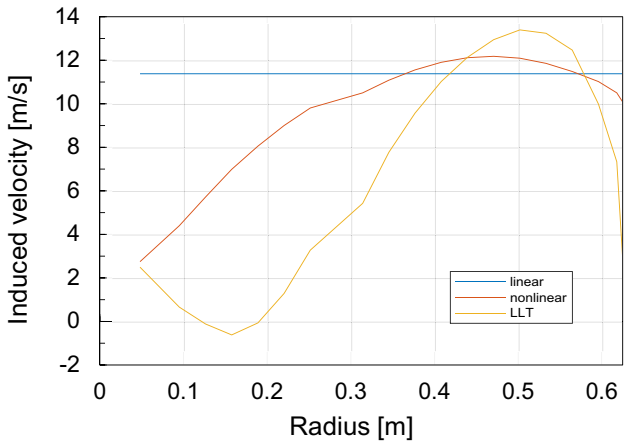

Fig. 32 H25F: induced velocity comparison in static operations: RPM 2500, $v_\infty = 1$ m/s

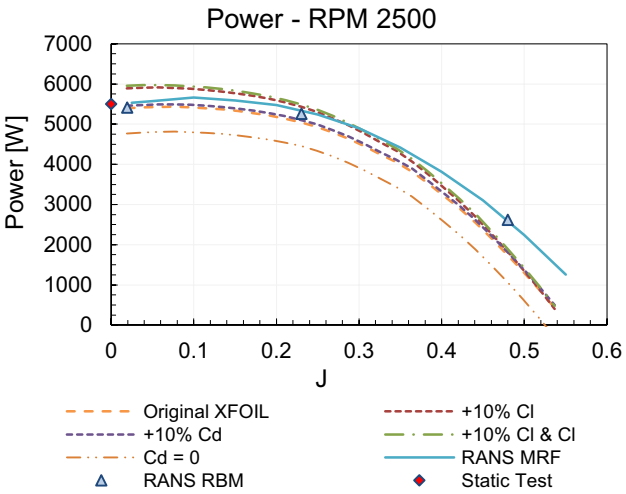

Fig. 34 H25F: influence of 2D data to power consumption change

continuously increases, and the drag is diverging. Evaluating JavaFoil and, respectively, JavaProp, shows massive c_l and c_d overprediction, resulting in massive thrust and power consumption errors.

5 Conclusions

The presented paper shows the advantaged and disadvantages of the open source propeller simulation tool. JavaProp is fast and provides some primary data, which could be used as an initial guess of power and thrust versus advance ratio. However, JavaProp also shows non-physical effects at low advance ratios and overpredicts thrust and power, which results from insufficient 2D airfoil data. The data import in XROTOR is complex, and the 2D polar points have to be calculated for arbitrary geometries without support or an appropriate interface. Therefore, XROTOR could be used in an advanced development environment but not for fast thrust or power predictions, even though the turnaround time is massively reduced due to the Fortran-based programming language. XROTOR has good thrust prediction capabilities, but power consumption prediction is less accurate. JBlade is outstanding in handling qualities and creates acceptable results at high advance ratios at an appropriate time, even for less expired users. The tool could be used standalone and need no other interfaces or tools. However, the wrong behaviour in low advance ratio conditions results in significant differences between JBlade and the MRF simulation. This error results from the post-stall model and the manipulation of the 2D airfoil data with the post-stall model. RAALF can be used for propeller simulations. Still, propeller simulations are not the main focus of this project which is more on VLM procedures and helicopter or multirotor simulations. PropCODE is a standalone Matlab tool, which can be used for holistic aerodynamic, aeroacoustic, and aeroelastic simulations. The advantage of PropCODE against the other environments is the capability to process CAD geometries to identify chord and twist distributions and calculate 2D aerodynamic data. Especially the twist distribution has to be as accurate as possible, because derivations in twist result in significant changes of thrust and power consumption.

In principle, BET can be used for power and thrust calculations in the early design stages. Expected relative errors are in the range of ± 10–20% relative to RANS prediction if a suitable BET method is used. The presented calculation methods show sufficient accuracy compared to MRF simulation and partly against static test data. Some general, comprehensive statements on propeller simulations are made in the following.

1. Moving reference frame simulations are sufficient for thrust and torque prediction of an open propeller in Star-CCM + and need only a small fraction of CPU time of rigid body motion simulations.
2. The necessary 2D data generation shall be performed with XFOIL instead of JavaFoil, because XFOIL is more sophisticated and matches trend and magnitude compared to wind tunnel tests better.
3. A nonlinear momentum approach instead of a linear momentum approach or an LLT procedure with a fixed wake model should be used for low advance ratio conditions. If a semi-prescribed wake model is available and simulation time is not an issue, the LLT procedure with a semi-prescribed wake model is superior.
4. A BET method, coupled with a linear momentum approach, XFOIL, and the Prandtl tip-loss correction model is sufficient for accurate thrust and power consumption calculations in high advance ratios for conventional straight propellers, as realised in PropCODE or RAALF.
5. Accurate 2D aerodynamic airfoil data is required for high thrust and power prediction accuracy. A parabolic approach leads to high errors in low advance ratio conditions.

Appendix

H25F two-bladed 1.25 m propeller

Velocity sweep at constant RPM of 1500.

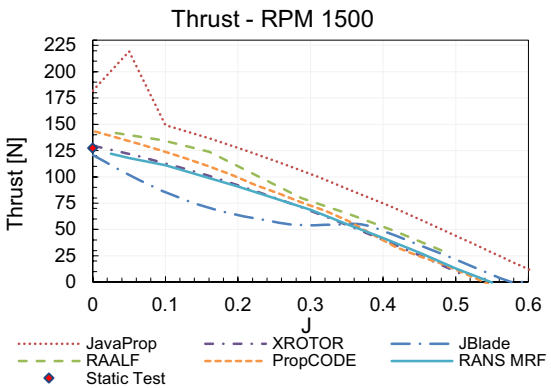

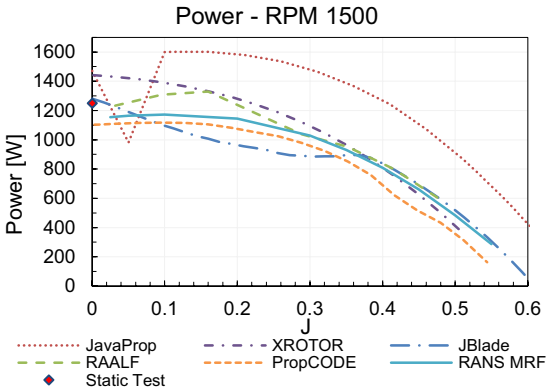

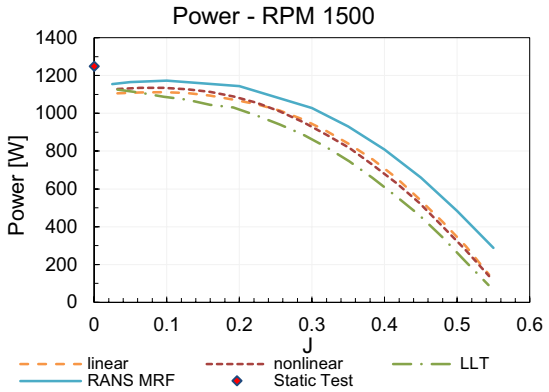

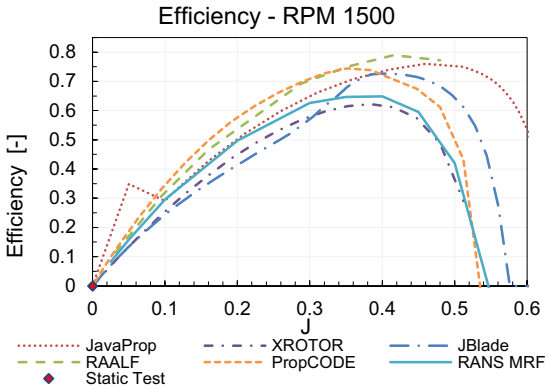

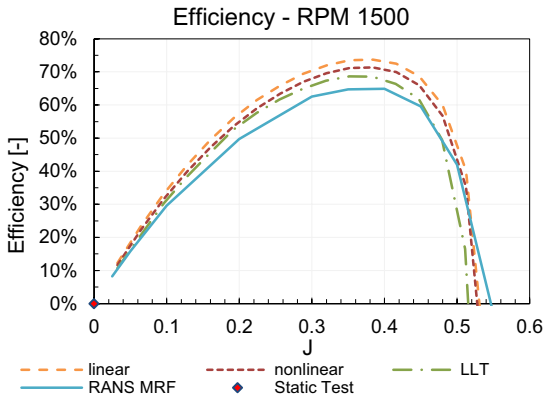

Velocity sweep at constant RPM of 1500: PropCODE.

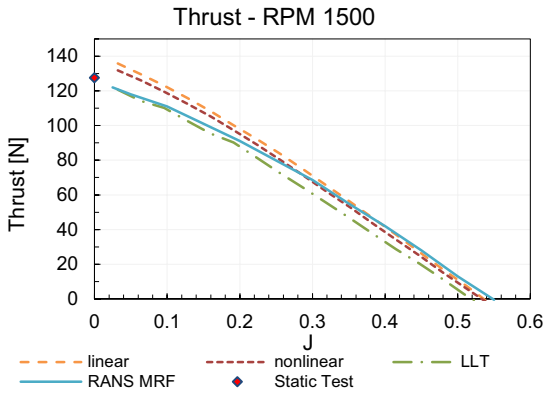

H30F three-bladed 1.60 m propeller

Velocity sweep at constant RPM of 2500.

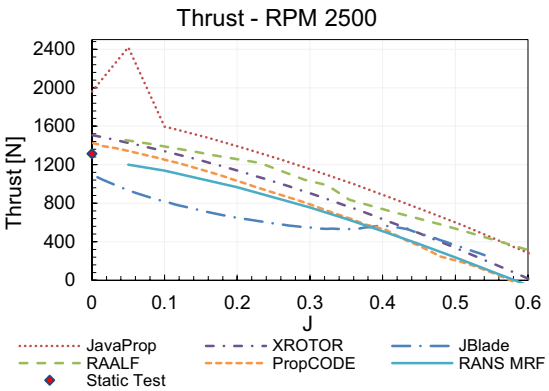

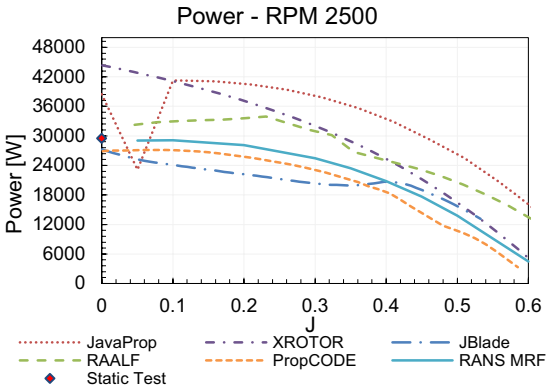

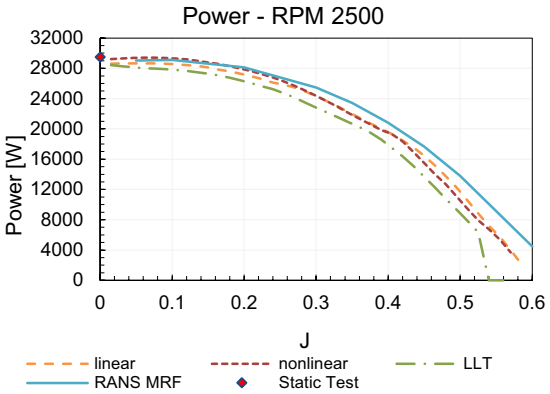

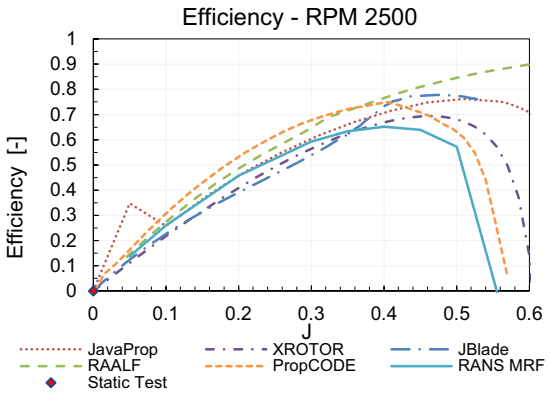

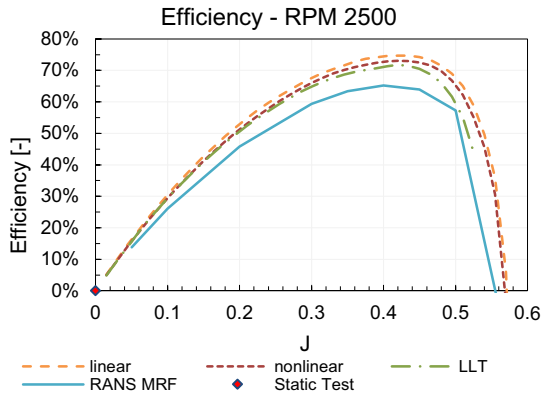

Velocity sweep at constant RPM of 2500: PropCODE.

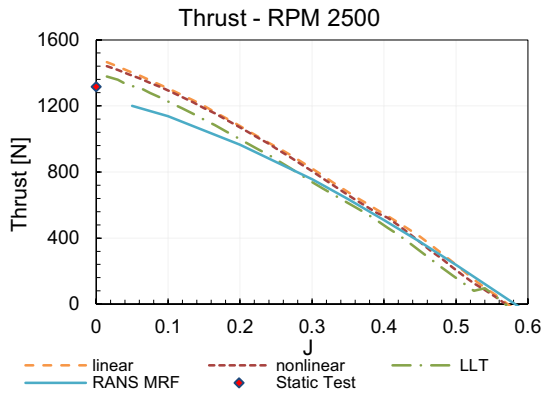

Acknowledgements The authors acknowledge the financial support by the Federal Ministry of Education and Research of Germany in the framework of IngenieurNachwuchs 2016 (project "DEFANA – Ducted Electric Fans for Novel Aircraft", project number 13FH638IX6). The authors like to express their gratitude to Siemens PLM Software for providing academic licenses of their software StarCCM+.

Funding Open Access funding enabled and organized by Projekt DEAL. Federal Ministry of Education and Research of Germany in the framework of IngenieurNachwuchs 2016 (project “DEFANA – Ducted Electric Fans for Novel Aircraft”, project number 13FH638IX6).

Availability of data and material Not applicable.

Code availability Not applicable.

Declarations

Conflict of interest Not applicable.

References

1. Grandl, G., Cachay, J., Salib, J.: The future of vertical mobility—a porsche consulting study (c) (2018)
2. Voskuijl, M., van Bogaert, J., Rao, A.G.: Analysis and design of hybrid electric regional turboprop aircraft. CEAS Aeron. J. **9**, 15–25 (2018)
3. Flightpath 2050: Europ's Vision for Aviation. Europe's vision for aviation ; maintaining global leadership and serving society's needs; report of the High-Level Group on Aviation Research. Policy / European Commission. Publ. Off. of the Europ. Union, Luxembourg
4. Finger, F.D., Braun, C., Bil, C.: Comparative assessment of parallel-hybrid-electric propulsion systems for four different aircraft. In: AIAA SciTech (2020)
5. Finger, D.F., Braun, C., Bil, C.: A review of configuration design for distributed propulsion transitioning VTOL aircraft. In: Asia Pacific International Symposium on Aerospace Technology (ed) APISAT (2017)
6. Aigner, B., Stumpf, E., Hinz, A., de Doncker, R.W.: An integrated design framework for aircraft with hybrid electric propulsion. In: AIAA Scitech Forum, Orlando, FL, Reston, Virginia. https://doi.org/10.2514/6.2020-1501 (2020)
7. Kwon, H.-I., Yi, S., Choi, S., Kim, K.: Design of efficient propellers using variable-fidelity aerodynamic analysis and multilevel optimization. J Propuls Power **31**(4), 1057–1072 (2005)
8. Gur, O., Lazar, G.: Prop-rotor design for an electric tilt-rotor vehicle. American Heli-copter Society, Future Vertical Lift Aircraft Design Conference, January 18–20, Fisherman's Wharf, San Francisco, California (2012)
9. Klesa, J.: Design of the propeller for tilt-rotor UAV. In: 20th International Conference Applied Mechanics, pp. 45–48 (2018)
10. Whitmore, S.A., Merrill, R.S.: Nonlinear large angle solutions of the blade element momentum theory propeller equations. J. Aircr. **49**(4), 1126–1134 (2012)
11. Carroll, J., Marcum, D.: Comparison of a blade element momentum model to 3d cfd simulations for small scale propellers. SAE Int. J. Aerosp. (2013). https://doi.org/10.4271/2013-01-2270
12. Chiew Jonathan, J., Aftosmis, M.J.: Efficient simulation of multirotor configurations with low Reynolds number propellers. AIAA AVIATION forum. In: AIAA aviation, p. 594 (2018)
13. Engineering Science Data Unit (ESDU): Approximate parametric method for propeller thrust estimation. ESDU 83001 (1983)
14. Engineering Science Data Unit (ESDU): Approximate parametric method for propeller thrust estimation. Appendum A: Application to Fixed-Pitch Propellers. ESDU 83028 (1983)
15. Hamilton Standard.: Generalized method of propeller performance estimation 1961–1963, Windsor locks, Connecticut (6101). https://hdl.handle.net/2144/10454 (1963)
16. Voskuijl, M.: Performance analysis and design of loitering munitions: a comprehensive technical survey of recent developments. In: Defence Technology (2021)
17. Voskuijl, M., Dekkers, T., Savelsberg, R.: Flight performance analysis of the samad attack drones operated by Houthi armed forces. In: Science & Global Security (2020)
18. Köhler, J., Jeschke, P.: Conceptual design and comparison of hybrid electric propulsion systems for small aircraft. CEAS Aircr. J. **12**(4), 907–922 (2021). https://doi.org/10.1007/s13272-021-00536-4
19. Hepperle, M.: Inverse aerodynamic design procedure for propellers having a prescribed chord-length distribution. J. Aircr. **47**, 1867–1872 (2010)
20. Drela, M., Youngren, H.: Axisymmetric analysis and design of ducted rotors, DFDC software manual (2005)
21. Silvestre, M.Â.R., Morgado, J., Pascoa, J.C.: JBLADE: a propeller design and analysis code. In: AIAA International Powerd Lift Conference, Los Angles, CA, p. 27. https://doi.org/10.2514/6.2013-4220 (2013)
22. Cole, J.A., Maughmer, M.D., Bramesfeld, G., Kinzel, M.: A higher-order free-wake method for propeller-wing systems. In: AIAA aviation, p. 31 (2017)
23. Klein, P.C.: Parametric modeling and optimization of advanced propellers for next-generation aircraft. Master Thesis, TU Delft university of Technology (2017)
24. Anemaat, W.A.J., van Dommelen, D., Johnson, S., Sargent, P.B., Liu, W.: Comparison of aerodynamic analysis tools for rotorcraft in hover. QProp FlightStream Star-CCM+. In: AIAA SciTech (2018)
25. Gur, O., Rosen, A.: Comparison between blade-element models of propellers. Aeron. J. **1138**, 689–704 (2008)
26. Morgado, J., Silvestre, M.Â.R., Páscoa, J.C.: Validation of new formulations for propeller analysis. J. Propul. Power (2015). https://doi.org/10.2514/1.B35240
27. Brandt, J.B., Selig Michael, S.: Propeller performance data at low Reynolds numbers. In: AIAA Aerospace Science Meeting, vol. 49, p. 141 (2011)
28. Mort, K.W., Gamse, B.: A wind-tunnel investigation of a 7-foot-diameter ducted propeller. NASA TN D-4142. NASA Ames Research Center (1967)
29. Theodorsen, T., Stickle, G.W., Brevoort, M.J.: Characteristics of six propellers including the high-speed range. NACA TR 594. NACA (1937)
30. Maynard, J.D., Salters, L.B. Jr.: Aerodynamic characteristics at high speeds of related full-scalce propellers having different blade-section Cambers. NACA Report 1309. NACA (1957)
31. McCrink, M.H., Gregory, J.W.: Blade element momentum modeling of low-reynolds electric propulsion systems. J. Aircr. (2017). https://doi.org/10.2514/1.C033622
32. Baltazar, J., Rijpkema, D., Falcao de Campos, J.A.C., Bosschers, J.: A comparison of panel method and rans calculations for a ducted propeller system in open water. In: Third International Symposium on Marine Propulsors (2013)
33. Montgomerie, B.: Methods for root effects, tip effects and extending the angle of attack range to ± 180°. FOI-R 1305 Sed, Stockholm, Schweden (2004)
34. Glauert, H.: Airplane propellers. In: Aerodynamic Theory, pp. 169–360. Springer, Berlin (1935). https://doi.org/10.1007/978-3-642-91487-4_3
35. Gur, O.: On the limits of blade-element model for high-pitch rotating wing. In: Israel Annual Conference on Aerospace Sciences (ed) IACAS, vol. 2020 (2020)

36. Rosen, A., Gur, O.: Propeller performance at low advance ratio. J. Aircr. (2005). https://doi.org/10.2514/1.6564
37. Hepperle, M.: JavaFoil—analysis of airfoils. https://www.mh-aerotools.de/airfoils/javafoil.htm (1996). Accessed 25 Feb 2021
38. Drela, M.: XFOIL: an analysis and design system for low Reynolds number airfoils. In: Low Reynolds Number Aerodynamics, vol. 54. Springer (1989)
39. Eppler, R., Somers, D.M.: A computer program for the design and analysis of low-speed airfoils. TM 80210. NASA Langley Research Center, Hampton, VA (1980)
40. Eppler, R., Somers, D.M.: Supplement to: a computer propgram for the design and analysis of low-speed airfoils, NASA Langley Research Center (1980)
41. Drela, M., Youngren, H.: XROTOR user guide. https://web.mit.edu/drela/Public/web/xrotor/xrotor_doc.txt (2003). Accessed 14 June 2021
42. Glauert, H.: The effects of compressibility on the lift of an aerofoil. Proc. R. Soc. Lond. Ser. A Math. Phys. Sci. **118**, 113–119 (1928)
43. Howe, D.: Aircraft Conceptual Design Synthesis. Professional Engineering Publishing Limited, Bury St Edmunds (2000)
44. Götten, F., Finger, F., Havermann, M., Braun, C., Marino, M., Bil, C.: A highly automated method for simulating airfoil characteristics at low Reynolds number using a RANS—transition approach. In: Deutsche Gesellschaft für Luft und Raumfahrt (ed) DLRK (2019)
45. Rogers, S.E., Roth, K., Nash Steven, M.: CFD validation of high-lift flows with significant wind-tunnel effects. In: AIAA Applied Aerodynamics Conference, Denver, Colerado (2000)
46. Smith, J.L., Graham, H.Z., Smith, J.E.: Validation of an airfoil in the ground effect regime using 2-D CFD analysis. In: AIAA Applied Aerodynamics Conference, Seattle, WA (2008)
47. Götten, F., Marino, M., Bil, C.: A review of guidelines and best practices for subsonic aerodynamics simulation using RANS CFD. In: Asia Pacific International Symposium on Aerospace Technology (ed) APISAT (2019)
48. Menter, F.R.: Two-equation eddy-viscosity turbulence models for engineering applications. AIAA J. (1994). https://doi.org/10.2514/3.12149
49. Menter, F.R., Smirnov, P.E., Liu, T.A., Avancha, R.: A One-Equation Local Correlation-Based Transition Model. In: Springer Science (ed) Flow turbulence Combust (2015)
50. Nicks, O., Steen, G., Heffner, M., Bauer, D.: Wind tunnel investigation and analysis of the SM701 airfoil. In: XXII OSTIV Congress, Uvalde, Texas (1991)
51. Althaus, D., Wurz, W.: Wind tunnel tests of the SM701 airfoil abd the UAG 88-143/20 airfoil. In: Technical Soaring. An international Journal, vol. XVII, no. 1 (1993)
52. Bertagnolio, F.: NACA0015 measurements in LM wind tunnel and turbulence generated noise. Risoe-R: no. 1657, Technical University of Denmark (2008)
53. Drela, M., Giles, M.B.: Viscous-inviscid analysis of transonic and low Reynolds number airfoils. AIAA J. **25**(10), 1347–1355 (1987)
54. Larrabee, E.E.: Practical design of minimum induced loss propellers, MIT Massachuestts Institude of Technology (1980)
55. Adkins, C.N., Liebeck, R.H.: Design of optimum propellers. J. Propuls. Power **10**(10), 676–682 (1994)
56. Betz, A., Prandtl, L.: Vier Abhandlungen zur Hydrodynamik und Aerodynamik, vol. 3. Universitätsverlag Göttingen, Göttingen (1919)
57. Eppler, R., Hepperle, M.: A procedure for propeller design by inverse methods, Universität Stuttgart (1984)
58. Goldstein, S.: On the vortex theory of screw propellers. By Goldstein, St. John's College; Kaiser Wilhelm-Institut für Strömungsforschung in Göttingen (1929)
59. Morgado, J.: Development of an open source software tool for propeller design in the MAAT project. Doctorial Theisis, University of Beira Interior (2016)
60. Morgado, J., Silvestre, M.Â.R., Páscoa, J.C.: A comparison of post-stall models extended for propeller performance prediction. Aircr. Eng. Aerosp. Technol. Int. J. **88**(4), 540–549 (2016)
61. Spera, D.A.: Models of lift and drag coefficients of stalled and unstalled airfoils in wind turbines and wind tunnels. NASA/CR-2008-215434. Jacobs Technology, Inc (2008)
62. Kolaei, A., Barcelos, D., Bramesfeld, G.: Experimental analysis of a small-scale rotor at various inflow angles. Int. J. Aerosp. Eng. (2018). https://doi.org/10.1155/2018/2560370
63. Cole, J.A., Krebs, T., Barcelos, D., Yeung, A., Bramesfeld, G.: On the integrated aerodynamic design of a propeller-wing system. In: AIAA SciTech, p. 31 (2019)
64. Bramesfeld, G.: A higher order vortex-lattice method with a force-free wake. Doctorial Theisis, Pennsylvania State University (2006)
65. Gur, O., Rosen, A.: Calculating the performance of fixed pitch propellers at low advance ratios. In: Israel Annual Conference on Aerospace Sciences. IACAS (2003)
66. Mahmuddin, F.: Rotor blade performance analysis with blade element momentum theory. In: 8th International Conference of Applied Energy. ICAE, pp. 1123–1129 (2016)
67. Montgomery, Z.S.: A propeller model based on a modern numerical lifting-line algorithm with an iterative semi-free wake solver. Master Theisis, Utah State University (2018)
68. Simcenter Star-CCM+. Documentation. Siemens
69. Ruiz, M.C.: CFD simulation of propellers: best practices analysis. Tesi di Laurea Magistrale, Politecnico di Torino (2019)
70. Spalart, P.R.: Strategies for turbulence modelling and simulations. Int. J. Heat Fluid Flow **21**, 252–263 (2000)
71. Spalart, P.R., Rumsey, C.L.: Effective inflow conditions for turbulence models in aerodynamic calculations. AIAA J. **45**(10), 2544–2553 (2007)
72. Kaya, D.: Estimation of aerodynamic loads of a propeller though improved blade element and momentum theory and propeller deisign optimization. Doctoral Thesis, Middle East Technical University (2021)